Analyzing a suitable elastic geomechanical model for Vaca Muerta Formation

Agustin Sosa Massaro [a, *], D. Nicolas Espinoza [b], Marcelo Frydman [c], Silvia Barredo [a], Sergio Cuervo [d]

[a] Department of Petroleum at Instituto Tecnológico de Buenos Aires (ITBA), Buenos Aires, Argentina
[b] Department of Petroleum and Geosystems Engineering, The University of Texas at Austin, USA
[c] Schlumberger Technology Integration Center, Buenos Aires, Argentina
[d] Unconventional Resources - Asset Development Team, Chevron, Houston, USA

Keywords:
Elastic geomechanical model
Vaca Muerta Formation
Heterogeneity
VTI
Anisotropy

A B S T R A C T

Accurate geomechanical evaluation of oil and gas reservoir rocks is important to provide design parameters for drilling, completion and predict production rates. In particular, shale reservoir rocks are geologically complex and heterogeneous. Wells need to be hydraulically fractured for stimulation and, in complex tectonic environments, it is to consider that rock fabric and *in situ* stress, strongly influence fracture propagation geometry.

This article presents a combined wellbore-laboratory characterization of the geomechanical properties of a well in El Trapial/Curamched Field, over the Vaca Muerta Formation, located in the Neuquén Basin in Argentina. The study shows the results of triaxial tests with acoustic measurements in rock plugs from outcrops and field cores, and corresponding dynamic to static correlations considering various elastic models. The models, with increasing complexity, include the Isotropic Elastic Model (IEM), the Anisotropic Elastic Model (AEM) and the Detailed Anisotropic Elastic Model (DAEM).

Each model shows advantages over the others. An IEM offers a quick overview, being easy to run without much detailed data for heterogeneous and anisotropic rocks. The DAEM requires significant amounts of data, time and a multidisciplinary team to arrive to a detailed model. Finally, an AEM suits well to an anisotropic and realistic rock without the need of massive amounts of data.

1. Introduction

Shales are one of the most abundant sedimentary rocks in the earth's crust and constitute a large proportion of the clastic fill in sedimentary basins. In petroliferous hydrocarbon bearing basins, organic shales are the source rock for gas and petroleum generation and shales of all types can be seals to traps (Kuila et al., 2010). In Argentina, the Vaca Muerta Formation, located in the Neuquén Basin, is growing in economic importance, being the second largest shale gas in proven reserves, and the fourth largest with respect to oil, according to the US Energy Information Administration (EIA, 2014 reports).

Shale formations exhibit anisotropic properties due to their intrinsic lamination at various scales as well as the existence of microfractures at preferred orientations. Moreover, they exhibit large spatial heterogeneity because of the change in properties in all direction, meaning that the material properties change by location, especially in vertical direction (Mokhtari et al., 2014a,b). Anisotropy and heterogeneity affect various properties of shales such as tensile strength (Mokhtari et al., 2014a,b), compressive strength (Mokhtari et al., 2013a), permeability (Tutuncu and Mese, 2011; Tutuncu, 2012; Mokhtari et al., 2013b) and elastic (sonic) properties (Thomsen, 1986; Vernik and Nur, 1992; Wang, 2002; Tutuncu, 2010, 2012; and Mese and Tutuncu, 2011).

Due to the anisotropy and heterogeneity, shale reservoirs, require detailed geomechanical characterization to obtain cost-effective drilling, completion and production. The degree of anisotropy or heterogeneity in transport and mechanical properties can result in different implications (Mokhtari et al., 2014a,b). Havens (2011), demonstrated how considering mechanical anisotropy could improve the estimation of minimum horizontal stress in the Bakken shale. Serejian and Ghassemi (2011) determined the

* Corresponding author.
E-mail address: sosamassaroagustin@gmail.com (A. Sosa Massaro).

effect of mechanical anisotropy on fracture initiation pressure. Chertov (2012) proposed an equation to calculate fracture width in transversely isotropic media and compared the results with the conventional equation of Sneddon for isotropic media. Lee et al. (2012) demonstrated how the direction of breakout and wellbore stability analyses could be affected by anisotropic mechanical properties. Maxwell (2009) discussed the effect of anisotropy-derived uncertainties in the sonic velocity model on microseismic modeling. Additionally, it is worth mentioning that anisotropic and heterogeneous transport properties of shale reservoirs impart drastic changes in production simulation models (Mohaghegh, 2013).

Mechanical parameters obtained in the laboratory can be used to calibrate wellbore geomechanical models. Knowledge of the mechanical properties such as elastic and strength parameters and the *in situ* stresses of the subsurface formations are essential to face wellbore stability problems, fracturing operations, subsidence problems and sand production evaluation.

Mechanical anisotropy in shales has been widely reported in the laboratory, for both static (Amadei, 1996; Suarez-Rivera et al., 2011) and dynamic conditions (Wang, 2001), and it can be as high as 400% for horizontal over vertical Young's moduli (Eh/Ev). Anisotropy in the Vaca Muerta Formation can be as high as 250% (Frydman et al., 2016), while in the study zone, anisotropy has been reported to be near 40% (Cuervo et al., 2014). If isotropic properties are assumed in mechanical models, one may underestimate the true horizontal elastic properties of the formation and consequently the magnitude of horizontal stresses (Cuervo et al., 2014; Frydman et al., 2016; among others).

To properly characterize anisotropy in the Vaca Muerta Formation over the study area (Fig. 1), local correlations were developed between dynamic properties and their static equivalents from available laboratory data. The static elastic moduli were measured using axial deviatoric loading. The dynamic elastic moduli were measured using an ultrasonic pulser/receiver, measuring velocities in different directions to obtain the five independent stiffness coefficients C_{11}, C_{13}, C_{33}, C_{44} and C_{66} to fully characterize the geomechanical properties of vertical transverse isotropic (VTI) model (Fjaer et al., 2008).

This work also synthetizes how to deal with complexity varying elastic models, and with different amounts of data. The challenge will be to identify strengths and weaknesses in an Isotropic Elastic Model (IEM), an Anisotropic Elastic Model (AEM), or the special case of an AEM, the Detailed Anisotropic Elastic Model (DAEM), with lithological discrimination. Each model will display the better-suggested applications depending on the job.

2. Geological setting

The Vaca Muerta Formation is a thick Upper Jurassic unit that extends over 25,000 km^2 in the Neuquén Basin. It represents the most important source rock in Argentina and is presently a key unconventional reservoir for economic development. The Neuquén basin corresponds to a continental back-arc rift related to the Gondwana subductive margin that was characteristically connected with the Paleo-Pacific Ocean permitting several marine ingressions across the magmatic arc (Gulisano et al., 1984; Mitchum and Uliana, 1985; Legarreta and Gulisano, 1989; Legarreta et al., 1993). The marine source rocks of this unit were deposited during a period of early post-rift and long-term sea level highstands driven by sea-level oscillations and minor tectonic influence (Barredo and Stinco, 2013). The resulting high accommodation space and cyclic nature of the deposits provided the proper marine environment conditions to promote the development of the Vaca Muerta thick and proliferous source rock. Geochemical data shows that it has a TOC that varies from 3% to 8%, Ro_{max} 0,8%–2%, Hydrogen Index 400 to 800 mgHC/gTOC, SPI 5 to 20 tHC/m^2, kerogen type I-II and IIS in marginal areas, and VKA of high quality amorphous (Stinco and Mosquera, 2003; Legarreta and Villar, 2011; Barredo and Stinco, 2013).

The succession consists of low-energy, deep-water black shales with isolated sandy gravitational flow deposits in the western and middle sections of the basin that passes laterally and to the east to calcareous sandstones, marls and limestones. Productive levels are characterized by a stacked rhythmic alternation of marls, organic-rich shales and limestones related to an external ramp with restricted conditions (Spalletti et al., 2000; Scasso et al., 2002; Stinco and Mosquera, 2003; among others). Towards the basin border these facies interfinger with proximal westward prograding sandstones (Mitchum and Uliana, 1985; Legarreta and Gulisano, 1989).

Local controls in deposition existed because ancient extensional faults were still active presumably under late elastic relaxation (Stinco and Barredo, 2014a). However, the notable high frequency cyclicity of this formation is associated with systematic changes in productivity on the sea surface, and supply of terrigenous and non-terrigenous material in suspended plumes under Milankovitch cycle range (Stinco and Mosquera, 2003; Kietzmann et al., 2008; among others). These tectonic and eustatic controls left behind a series of heterogeneous rocks that vertically and laterally comprises a wide variety of lithologies: shales, marls, carbonates, calcareous sandstones and sandstones (Fig. 2) being carbonates most developed in proximal areas. Organic matter content increases at the

Fig. 1. Work area location. El Trapial/Curamched Fields to the east (yellow polygon) and Yesera del Tromen/Puerta Curaco outcrops to the west (in green). (For interpretation of the references to colour in this figure legend, the reader is referred to the web version of this article.)

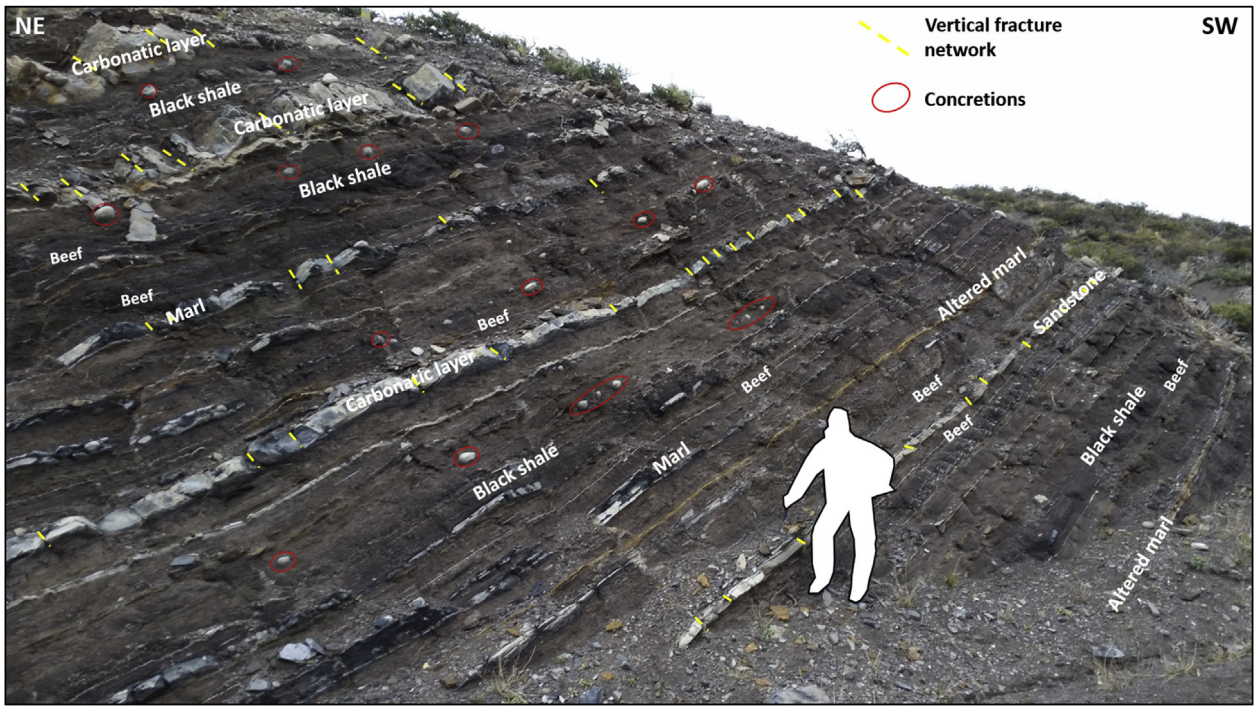

Fig. 2. Photography showing the general aspect of the lower Vaca Muerta Formation in Yesera del Tromen outcrop.

base of the formation suggesting maximum height of the water level.

In the study area, detailed analysis of the rocks shows that limestones are argillaceous, dominated by bioclastic mudstones, wackestones, packstones, floatstones and rudstones. Mineralogy consists of fractions of quartz, calcite and low percentage of clay (mainly illite and glauconite). Alternating coarse and fine beds in the shales results in thinly laminated bodies sometimes disturbed by bioturbation, concretions and bedding-parallel veins of fibrous calcite (beef) (Rodrigues et al., 2009). There are also low-angle cross-stratified and massive poorly stratified siltstones. Natural micro-cracks and certain mineral grain orientation can also be observed in coarser shales or laminated wakestones (Fig. 3a and b).

Limestones comprise massive to poorly stratified, bioclastic mudstones and wackestones, thinly laminated marls, and rippled laminated packstones (Fig. 3c). Those facies also underwent post-depositional dissolution processes that gave place to the formation of rims and holes and were also affected by fracturing in outcrop and well (Fig. 3d and e).

Finally, it is worth mentioning that the Vaca Muerta Formation exhibits overpressure gradients. Published data suggests a range from 0.50 psi/ft in the basin border to 1.10 psi/ft in the center of the basin (Askenazi et al., 2013). This overpressure suggests high hydrocarbons storage capacity, easy reservoir stimulation (due to effective stress reduction) and easy fluid recovery.

3. Methods and results

Triaxial tests over a wide variety set of plugs were carried out in UT (University of Texas at Austin) to understand and measure the mechanical anisotropy of rocks from the Vaca Muerta Formation. The triaxial frame used in the laboratory, displays similar characteristics of those used in commercial laboratories. It permits testing at high confining pressures (up to 20 KPSI) and controlling the axial stress until peak deviatoric stress (axial load up to 500,000 Lbs). High stiffness of the load frame provides strain control close to and after failure in strain-softening materials. Samples were loaded between two endcaps, each equipped with three piezoelectric transducers for measuring propagation of compressional P waves and shear S waves at 90° Sx and Sy. First arrivals were picked using a multi-window time averaging algorithm, which detects amplitude spikes above a predetermined threshold. Elastic wave velocities were calculated from arrival times after being corrected for endcap travel, and local strains calculated from axial and radial displacements measured through a set of sample-mounted cantilever arms. The equipment also measures pore pressure and temperature.

The tests performed in the laboratory considered three preferential directions, in this case, perpendicular (vertical), parallel (horizontal) and at 45° to the lamination of the rock obtained from extracted field cores of the Well-1, corresponding to El Trapial/Curamched Field. Deviatoric loading tests without and with confining stress (single and multiple stage) were performed with strain and ultrasonic velocity measurement. The results were used to obtain an estimation of the anisotropic elastic properties (dynamic and static) in order to develop correlations and set calibration points.

All of these tests allow to calculate the static and dynamic elastics properties (stiffness, Young's modulus, Poisson ratio, shear modulus and bulk modulus) and strength properties (friction angle, unconfined compressive strength and cohesive strength). It is worth mentioning that properties calculated for Well-1 derive from the core analysis of three wells in El Trapial/Curamched area, and have been contrasted with several measurements carried on in outcrop samples from the areas depicted in Fig. 1. Modulus from Well-1 exhibited similar values from those of the neighboring wells and higher values than those from outcrops (likely due to physical and chemical alterations produced by the uplift of the fold and a thrust belt to the west). Wells have been vertically drilled, and for the simplicity of the geomechanical model, layers from Well-1 are considered to be horizontal (core photographs Figs. 3c and 13) and so are the rock layers from the other wells despite the eastern ones

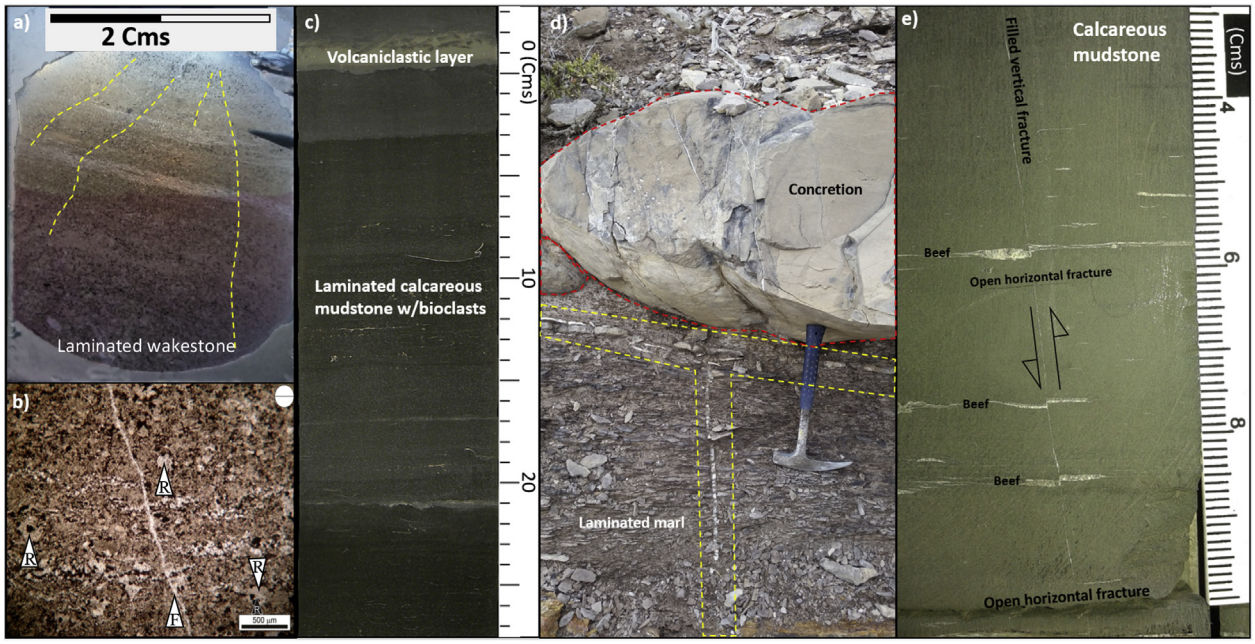

Fig. 3. Heterogeneity and rock complexity from Vaca Muerta Formation from outcrop and subsurface core. a) Thin section from a horizontal plug taken from outcrop. b) Microphotograph in crossed polars from figure a), showing alternating micritic and pseudoesparitic layers with calcitic radiolars (R), microcracks filled with calcite and/or gypsum with granular texture (F) and terrigenous. c) Core showing high heterogeneity due to a laminated calcareous section, note that the sheets do not exceed a centimeter thick. d) "T" shaped fracture growing across the highly laminated marl until split in two branches against the concretion. e) Calcareous mudstone from core, showing a homogeneous lithology with randomly horizontal and vertical distributed beefs, open fractures and vertical filled fractures, that impart a strong heterogeneity to this section.

gently deep to the east, and the western ones deep to the west, as a consequence of the northeast to southwest Chihuido de la Sierra Negra Anticline.

3.1. Elastic geomechanical model

The simplest strain-stress model assumes a linear relationship between stresses and the corresponding deformations (Fig. 4). Under certain conditions, rock behavior may follow the linear elastic assumption, such as when the applied stress is sufficiently small and the deformations are recoverable (Winkler et al., 1998). For example, elastic wave propagation in rocks can be studied using the linear elastic assumption (Mavko et al., 1995).

The theory of linear elasticity states that strain and stresses are related through a proportionality factor as:

$$\sigma_{ij} = C_{ijkl} \cdot \varepsilon_{kl} \tag{1}$$

$$\varepsilon_{ij} = S_{ijkl} \cdot \sigma_{kl} \tag{2}$$

where C_{ijkl} is known as the stiffness tensor, S_{ijkl} is the compliance tensor ($S_{ijkl} = C_{ijkl}^{-1}$), σ is the stress tensor, and ε is the strain tensor. Using the stress tensor symmetry, it is possible to reduce the constant number of the fourth-order tensor (C_{ijkl}) that are necessary to describe the elastic properties of a material. In this way, the number of constants from 81 is reduced to 54 (Radovitzky, 2003). Similarly, we can use the symmetry of the strain tensor to reduce the number of material constants to 36. Elastic material symmetry must be considered to further reduce the number of material constants. The most general, linear elastic anisotropic material, has 21 constants. Using the Voigt notation (Voigt, 1928), where $C_{ijkl} = C_{\alpha\beta}$, the following matrix is obtained (with values "0" equivalent to the symmetry of the matrix) (Thomsen, 1986; Radovitzky, 2003; among others):

$$\begin{bmatrix} \sigma_{11} \\ \sigma_{22} \\ \sigma_{33} \\ \sigma_{23} \\ \sigma_{13} \\ \sigma_{12} \end{bmatrix} = \begin{bmatrix} C_{11} & C_{12} & C_{13} & C_{14} & C_{15} & C_{16} \\ 0 & C_{22} & C_{23} & C_{24} & C_{25} & C_{26} \\ 0 & 0 & C_{33} & C_{34} & C_{35} & C_{36} \\ 0 & 0 & 0 & C_{44} & C_{45} & C_{46} \\ 0 & 0 & 0 & 0 & C_{55} & C_{56} \\ 0 & 0 & 0 & 0 & 0 & C_{66} \end{bmatrix} = \begin{bmatrix} \varepsilon_{11} \\ \varepsilon_{22} \\ \varepsilon_{33} \\ \varepsilon_{23} \\ \varepsilon_{13} \\ \varepsilon_{12} \end{bmatrix} \tag{3}$$

When the material presents symmetries in its structure, the number of material constants is further reduced. This is the case of the rocks of the Vaca Muerta Formation, where parallel (horizontal) and perpendicular (vertical) properties are different. Variations in mechanical properties are due to lithological vertical changes, ranging from millimeters to meters, also showing a wide variety of vertical to subhorizontal natural fractures, open, closed and mineral-filled (see Section 2). It is possible to utilize different elastic models to describe rock elastic behavior, such as the isotropic model and anisotropic models with their subtypes, namely VTI (Vertical Transverse Isotropy), HTI (Horizontal Transvere Isotropy) and Orthorhombic (Orthotropic) (Fig. 5). Among them, the VTI model is the most used in geomechanics due to its relative

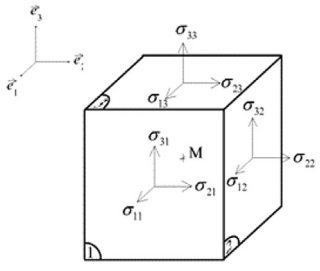

Fig. 4. Stress components acting on the 3-planes, where *e* is the strain and *σ* is the applied stress.

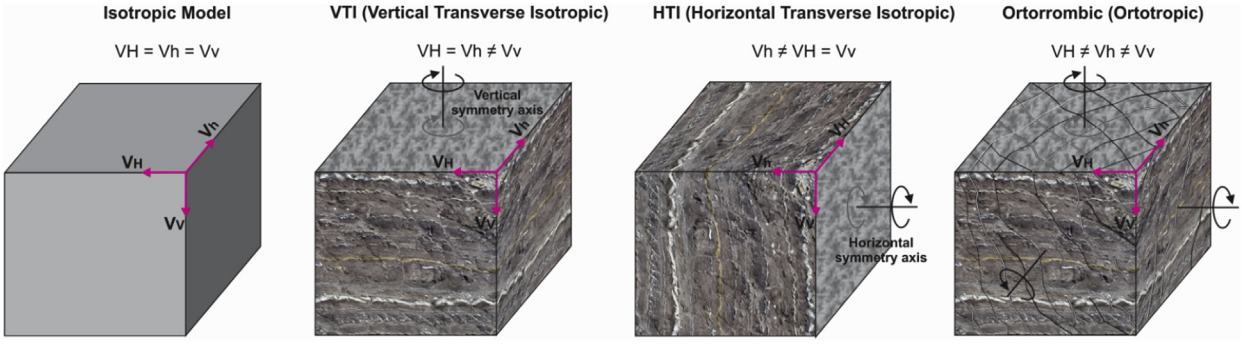

Fig. 5. Anisotropic mechanical models applicable to shale rocks like those found in Vaca Muerta Formation. Basic Isotropic Model; VTI Model, for horizontally laminated rocks; HTI Model, for laminated and steeply dipping rocks (vertical layers); and Orthorhombic Model, for combinations of natural fractures and multi layered rocks. References: V_V: Vertical Velocity, V_H: Horizontal Fast Velocity and V_h: Horizontal Slow Velocity.

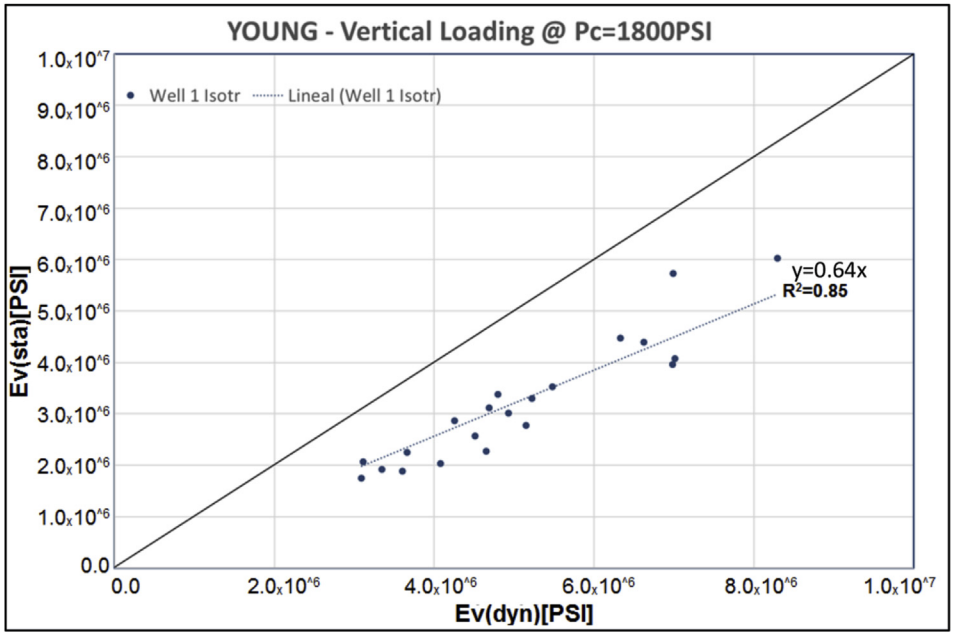

Fig. 6. Dynamic Vertical Young - Ev(dyn) Vs. Static Vertical Young - Ev(sta), at reservoir effective stress condition (confining pressure Pc = 1800 PSI).

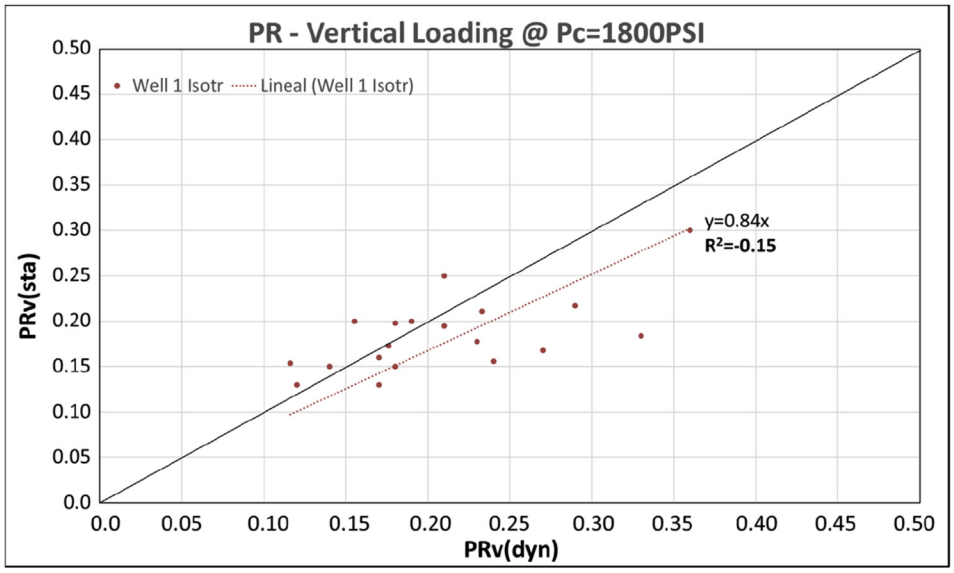

Fig. 7. Dynamic Vertical Poisson ratio - PRv(dyn) Vs. Static Vertical Poisson ratio - PRv(sta), at reservoir effective stress condition (confining pressure Pc = 1800 PSI).

mathematical simplicity (Thomsen, 1986). Anisotropy can be also associated with differences in horizontal and vertical stress directions and magnitudes, exerting their influence on both elastic isotropic media and VTI (Nur and Simmons, 1969; Rüger, 1996; among others).

3.1.1. Isotropic Elastic Model (IEM)

For isotropic media, the matrix takes the simplest form where the three-symmetry axes are taken as the unique axis:

$$\left[C_{\alpha\beta}\right] = \begin{bmatrix} C_{33} & (C_{33}-2C_{44}) & (C_{33}-2C_{44}) & 0 & 0 & 0 \\ 0 & C_{33} & (C_{33}-2C_{44}) & 0 & 0 & 0 \\ 0 & 0 & C_{33} & 0 & 0 & 0 \\ 0 & 0 & 0 & C_{44} & 0 & 0 \\ 0 & 0 & 0 & 0 & C_{44} & 0 \\ 0 & 0 & 0 & 0 & 0 & C_{44} \end{bmatrix} \tag{4}$$

To calculate the dynamic elastic modulus for an isotropic model, there is no need to calculate the $C_{\alpha\beta}$ stiff parameters. Dynamic moduli "G^{dyn}" and "K_b^{dyn}" are obtained from the relation between the rock bulk density ("ρ" *RHOB*) and the inverse of the compressional (V_p) and shear (V_s) velocities, Equations (5) and (6) (modified from Warpinski et al., 1998). Dynamic properties can be measured in the laboratory and around the well. "E^{dyn}" and "υ^{dyn}" can be calculated using Equations (7) and (8) (Thorne and Wallace, 1995).

The isotropic model is not the preferred model for highly heterogeneous rocks such as the Vaca Muerta Formation, due to its high level of mechanical anisotropy, as it has been demonstrated in previous works (Willis and Tutuncu, 2014; Frydman et al., 2016). If a geomechanical model requires celerity and data is scarce, an isotropic model could work as a first order approach, particularly in areas with weak anisotropy. Elastic parameters are usually best related in the vertical direction, hence, the calibration curve requires laboratory tests carried out in vertical plugs. This is due to the intrinsic nature of the propagation wave into the formation rock caused by emitter and receptor at the sonic tool (Haldorsen et al., 2006).

$$G^{dyn} = 13474,45.\frac{\rho}{DTSM^2} \tag{5}$$

$$K_b^{dyn} = 13474,45.\frac{\rho}{DTCO^2} - \frac{4}{3}.G^{dyn} \tag{6}$$

$$E^{dyn} = \frac{9G^{dyn}.K_b^{dyn}}{G^{dyn}+3K_b^{dyn}} \tag{7}$$

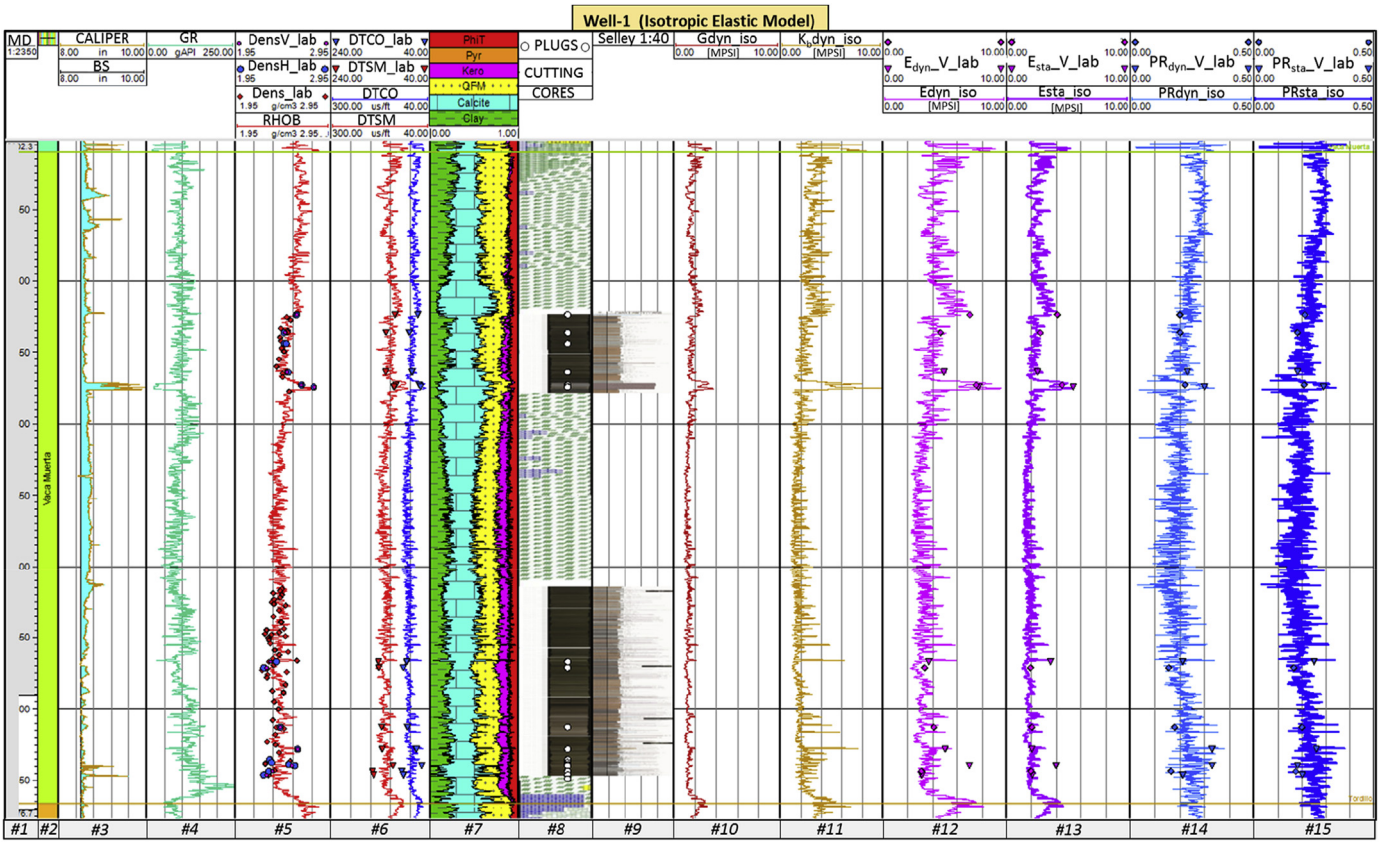

Fig. 8. Geomechanical Isotropic Elastic Model (IEM) for a heterogeneous rock. Dots over the curves represents the calibration points measured in vertical direction in laboratory. ***Track #1: MD***: *Measure Depth in meters;* ***#2***: *Vaca Muerta Formation;* ***#3: CALIPER*** *and* ***BS*** *(Bit Size) in inches;* ***#4: GR***: *Gamma Ray in gAPI;* ***#5: RHOB***: *Bulk Density in g/cm^3, with red and blue dots for laboratory calibration in vertical and horizontal plug direction;* ***#6: DTCO***: *Compressional Slowness and DTSM: Shear Slowness, both in us/ft;* ***#7***: *Petrophysics from gamma ray spectroscopy tool;* ***#8: CUTTING***: *Mudlogging, and* ***CORE***: *photographic core sections;* ***#9: Selley***: *Geological interpretation* log *(described by* Marlats and Tórtora, 2014*);* ***#10: G_{dyn}_iso***: *Dynamic Isotropic Shear Modulus in MPSI;* ***#11: Kb_{dyn}_iso***: *Dynamic Isotropic Bulk Modulus in MPSI;* ***#12: E_{dyn}_iso***: *Dynamic Isotropic Young Modulus in MPSI;* ***#13: E_{sta}_iso***: *Static Isotropic Young Modulus in MPSI;* ***#14: PR_{dyn}_iso***: *Dynamic Isotropic Poisson Ratio;* ***#15: PR_{sta}_iso***: *Static Isotropic Poisson Ratio. (For interpretation of the references to colour in this figure legend, the reader is referred to the web version of this article.)*

$$\upsilon^{dyn} = \frac{1}{2}\cdot\left(\frac{DTSM^2 - 2DTCO^2}{DTSM^2 - DTCO^2}\right) \quad (8)$$

where, G^{dyn} is the dynamic shear modulus (in MPSI), K_b^{dyn} is the dynamic bulk modulus (in MPSI), E^{dyn} is the dynamic Young's modulus (in MPSI), υ^{dyn} is the Poisson ratio, ρ is the formation rock density (in g/cm^3), *DTCO* is the compressional slowness (in μs/ft) and *DTSM* is the shear slowness (in μs/ft).

For completion purposes and others, geomechanical parameters must represent quasi-static deformation (static). Because of the small strain magnitudes involved in the passage of sonic waves (sonic logging) or ultrasonic waves (laboratory), dynamic measurements usually experience small strains, assuring purely elastic deformation (Sone, 2012). In contrast, quasi-static loading usually imparts much larger strain changes (e.g., on the order of 10^{-2}), which not only causes mineral elastic deformation but also induces inelastic deformation, such as frictional sliding and micro-crack growth, leading to pore structure changes (Zoback and Byerlee, 1975). As a consequence of the additional inelastic deformation captured in the static modulus measurements, the static Young's modulus is often lower than the dynamic modulus (Mavko et al., 2009). The static moduli are generally believed to be more representative of how an actual rock deforms under stress during drilling and completion in the field. Therefore, industry applications develop correlations between static and dynamic properties to infer reservoir deformation from well log-derived elastic properties (Hamza et al., 2015). Many correlations have been developed and applied for different basins around the world (Belikov, 1970; Gorjainov, 1979; Eissa, 1988; McCann, 1992; Morales and Marcinew, 1993; Lacy, 1997; Wang, 2000; Canady, 2010; among others), but it is relevant to mention, that each basin, each formation rock, and even each well, may present unique features.

Fig. 6 shows a good correlation (linear regression with $R^2 = 0.85$) between dynamic and static vertical Young's modulus measured on shales, marls and limestones from Well-1 in "as received" saturation conditions. In all cases, the static modulus is lower than the dynamic modulus. The obtained equation is extrapolated into the well in Fig. 8.

Poisson ratio correlation from vertical dynamic to static is considered to be the same (Morales and Marcinew, 1993; Barree and Gilbert, 2009). Fig. 7 shows that there is not a good correlation for Poisson ratio (linear regression with $R^2 = -0.15$), due to the mechanism used to test this type of rock in a triaxial test during the static measurements. A first hypothesis to understand this result is that the laminated nature of the rocks tested here could have controlled the development of microcracks along lamination planes, as has been noted by many other authors such as Barree and Gilbert. (2009).

Fig. 8 (tracks 3 to 9) shows the input data used to develop the geomechanical elastic model. Track 3 represents the bit size, together with the caliper log, a well logging tool that provides a continuous measurement of the size and shape of a borehole along its depth, where it is possible to see breakouts and washouts. Track

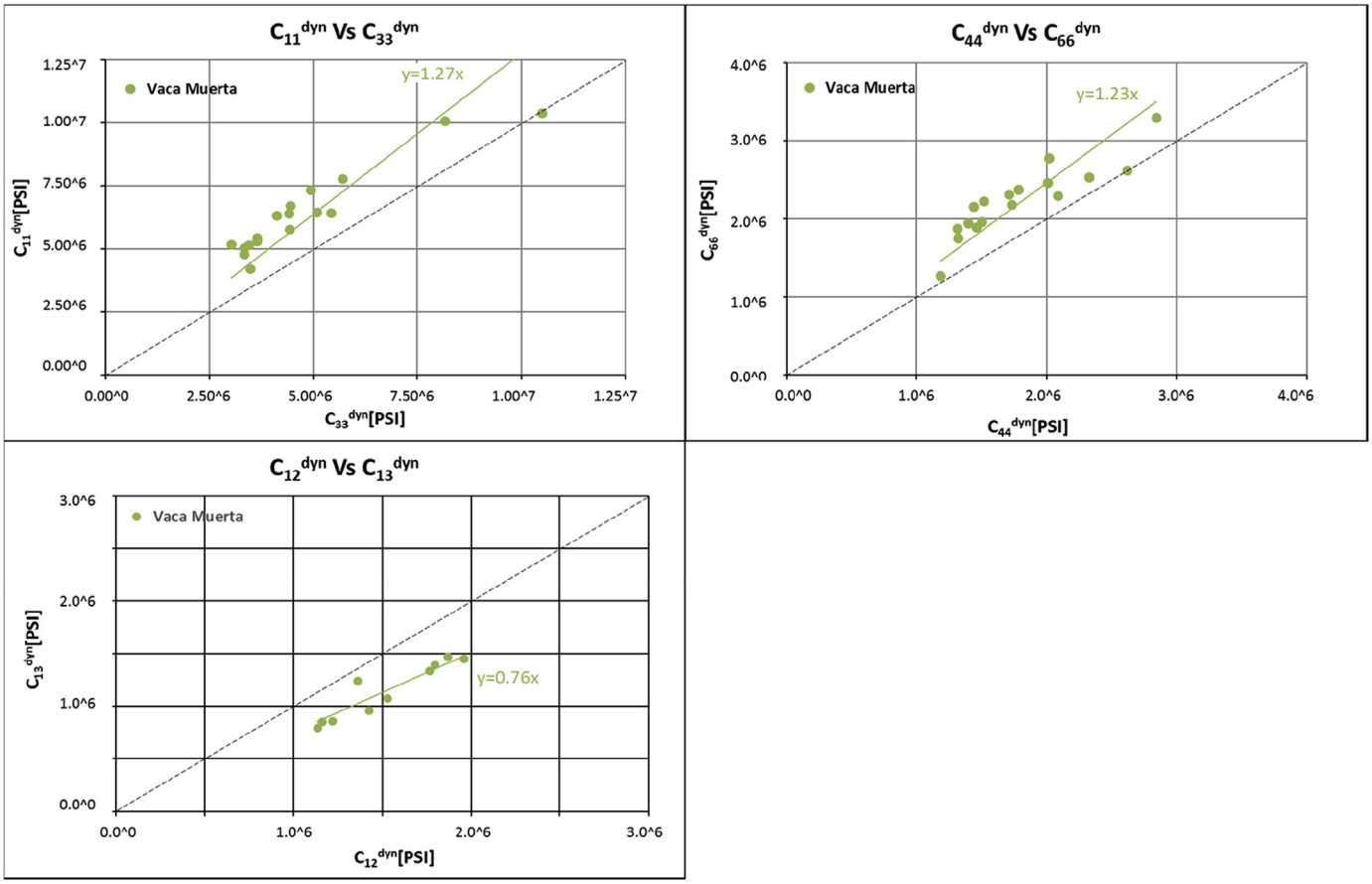

Fig. 9. C_{11}^{dyn}, C_{13}^{dyn}, C_{33}^{dyn}, C_{44}^{dyn} and C_{66}^{dyn}, represent the five independent dynamic elastic stiffness coefficients that characterize a transversely isotropic material. The correlations from linear regressions (with interception in "0") show good agreement between laboratory parameters, suggesting that it is possible to apply the same relations in the entire Vaca Muerta.

4 is the Gamma Ray (GR), useful to determine lithology from radioactive clay composition. Track 5 represents the bulk density (RHOB), showing good correlation with lab density measurements in vertical and horizontal samples. Track 6 represents the compressional (blue curve) and shear (red curve) slowness. As well as the density log, a good correlation with lab measurements is evident, where sample slowness seems to be slightly faster than well curves due to differences in wave frequency and vertical resolution. It is assumed that environmental corrections and calibrations have been properly applied to the well logs by the service company, and checked by the operator company. Tracks 7, 8 and 9 represent (in this order) the main mineralogical composition of the rocks interpreted from specialized well log measurements, the mud logging (cutting) together with pictures from the entire core, and finally the Selley log describing the core section.

The IEM shown in tracks 10 to 15 depicts the isotropic elastic behavior of the different lithologies along Vaca Muerta Formation. Good correlations between curves and laboratory measurements and correlations between dynamic to static were obtained. It must be remarked that this model gives a quick view of the rock behavior, mainly in the vertical direction, but not in the horizontal, as needed for describing and modeling an anisotropic environment.

3.1.2. Anisotropic Elastic Model (AEM)

The generalization carried from isotropy to transverse isotropy introduces three new elastic moduli. However, if the physical cause of the anisotropy is known, e.g., thin layering of certain isotropic media, these five moduli may not be independent after all (Thomsen, 1986). However, since the physical cause is rarely determined, the general treatment is a TIV Model, where as it going to be proved from triaxial testing, horizontal elastic properties are higher than vertical properties.

Horizontal symmetry in TIV media dictates:

$$C_{23} = C_{13}$$
$$C_{22} = C_{11}$$
$$C_{55} = C_{44}$$
$$C_{12} = C_{11} - 2C_{66}$$

$$\left[C_{\alpha\beta}\right] = \begin{bmatrix} C_{11} & (C_{11}-2C_{66}) & C_{13} & 0 & 0 & 0 \\ 0 & C_{11} & C_{13} & 0 & 0 & 0 \\ 0 & 0 & C_{33} & 0 & 0 & 0 \\ 0 & 0 & 0 & C_{44} & 0 & 0 \\ 0 & 0 & 0 & 0 & C_{44} & 0 \\ 0 & 0 & 0 & 0 & 0 & C_{66} \end{bmatrix} \quad (9)$$

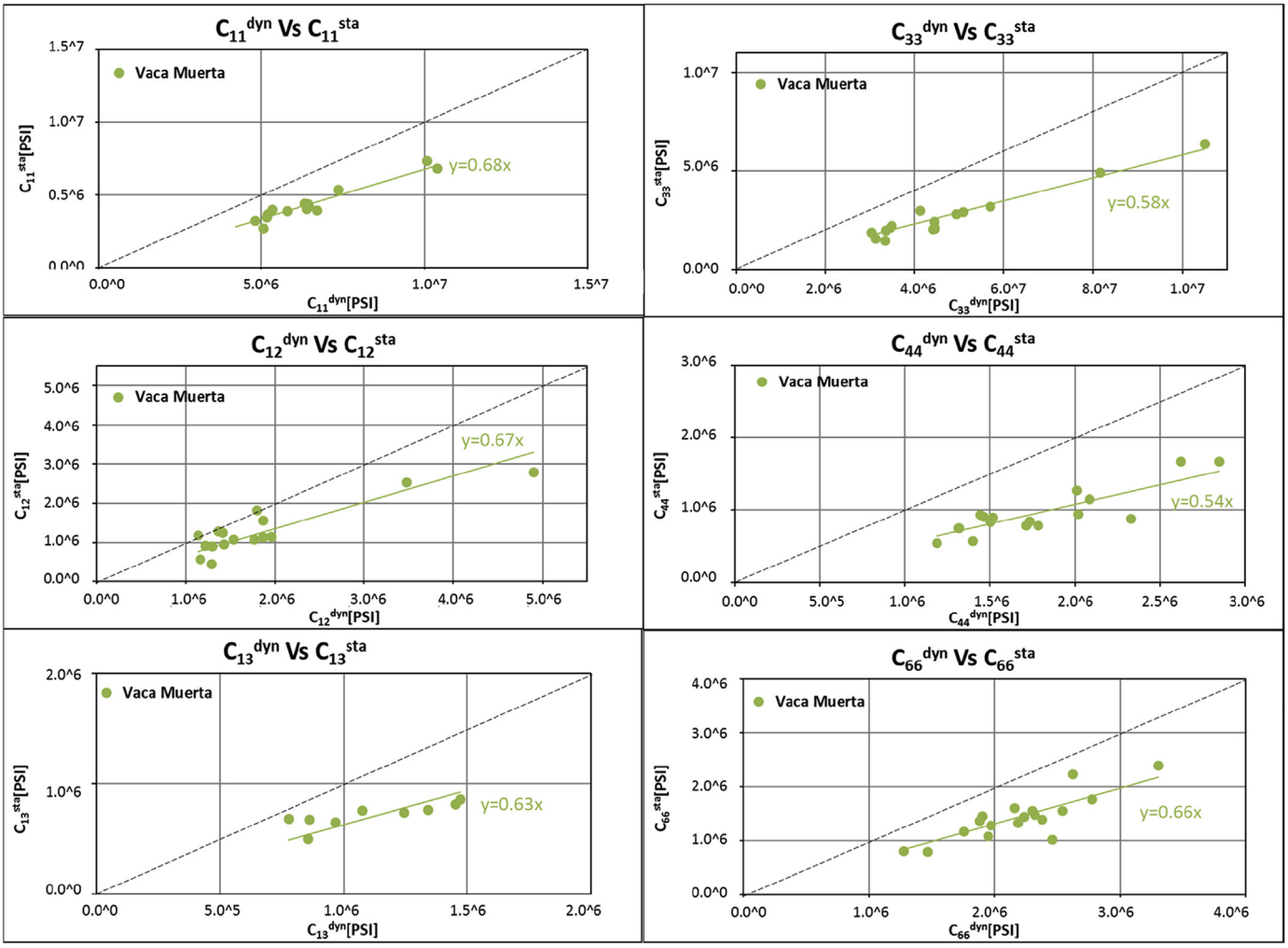

Fig. 10. Dynamic to Static correlations for C_{11}, C_{12}, C_{13}, C_{33}, C_{44} and C_{66}. The correlations from linear regressions (with interception in "0") fits well between laboratory parameters for C_{11}, C_{12}, C_{13}, C_{33}, C_{44} and C_{66}, meaning that it is possible to apply the same relations in the entire well.

The five independent dynamic stiffness coefficients ($C_{\alpha\beta}$) can be calculated from equations (10)–(14), while C_{12} is a function of C_{11} and C_{66} (in PSI units). This alternative can reduce the high dispersion found in calculating Poisson ratio and represents better the anisotropy in a TIV model.

$$C_{33}^{dyn} = 0.01347445\rho Vp^2(0^\circ) \tag{10}$$

$$C_{44}^{dyn} = 0.01347445\rho Vs^2(0^\circ) \tag{11}$$

$$C_{11}^{dyn} = 0.01347445\rho Vp^2(90^\circ) \tag{12}$$

$$C_{66}^{dyn} = 0.01347445\rho Vs^2(90^\circ) \tag{13}$$

$$C_{13}^{dyn} = C_{44}^{dyn} + 1/2\left[C_{11}^{dyn} + 2C_{44}^{dyn} + C_{33}^{dyn} - 4\rho 0.01347445\left(\mathrm{Vs}(45^\circ)^2\right)2 - \left(C_{11}^{dyn} - C_{33}^{dyn}\right)2\right]^{0.5} \tag{14}$$

$$C_{12}^{dyn} = C_{11}^{dyn} - 2C_{66}^{dyn} \tag{15}$$

where, $Vp(0^\circ)$ is the velocity of P-wave normal to bedding, $Vp(90^\circ)$ is the velocity of P-wave parallel to bedding, $Vs(0^\circ)$ is the velocity of S-wave normal to bedding, $Vs(90^\circ)$ is the velocity of S-wave parallel to bedding, $Vp(45^\circ)$ is the velocity of P-wave at 45° to bedding (all the velocities are in ft/μs), ρ is the bulk density (in g/cm^3) and 0.01347445 is a constant factor for converting units to PSI.

Fig. 9 displays the relationship between vertical and horizontal dynamic stiffness ($C_{\alpha\beta}^{dyn}$) without differentiation by lithofacies. Considering a vertical well, drilled perpendicular to bedding, $Vp(0^\circ)$ and $Vs(0^\circ)$ are obtained directly from sonic logging. Based on the correlations from Fig. 9, the full dynamic stiffness tensor is obtained (Equation (16)–(19)). The samples analyzed in the crossplots, have been selected at different depths for several lithologies (limestones [11%], calcareous mudstones [28%], slightly calcareous mudstone [33%] and mudstones [28%]) from a total of 367 mts core from three wells inside El Trapial and Curamched areas. The reservoir properties display clear differences for each section, including organic carbon richness and quantity of clays minerals. General trends in the lower section shows high total organic carbon, which decreases upwards, and carbonate content increasing upwards. In contrast, the upper section is poor in organic carbon content and clay (Fantin et al., 2014).

It is worth mentioning that a greater number of samples are required for representative correlations, reducing statistical errors.

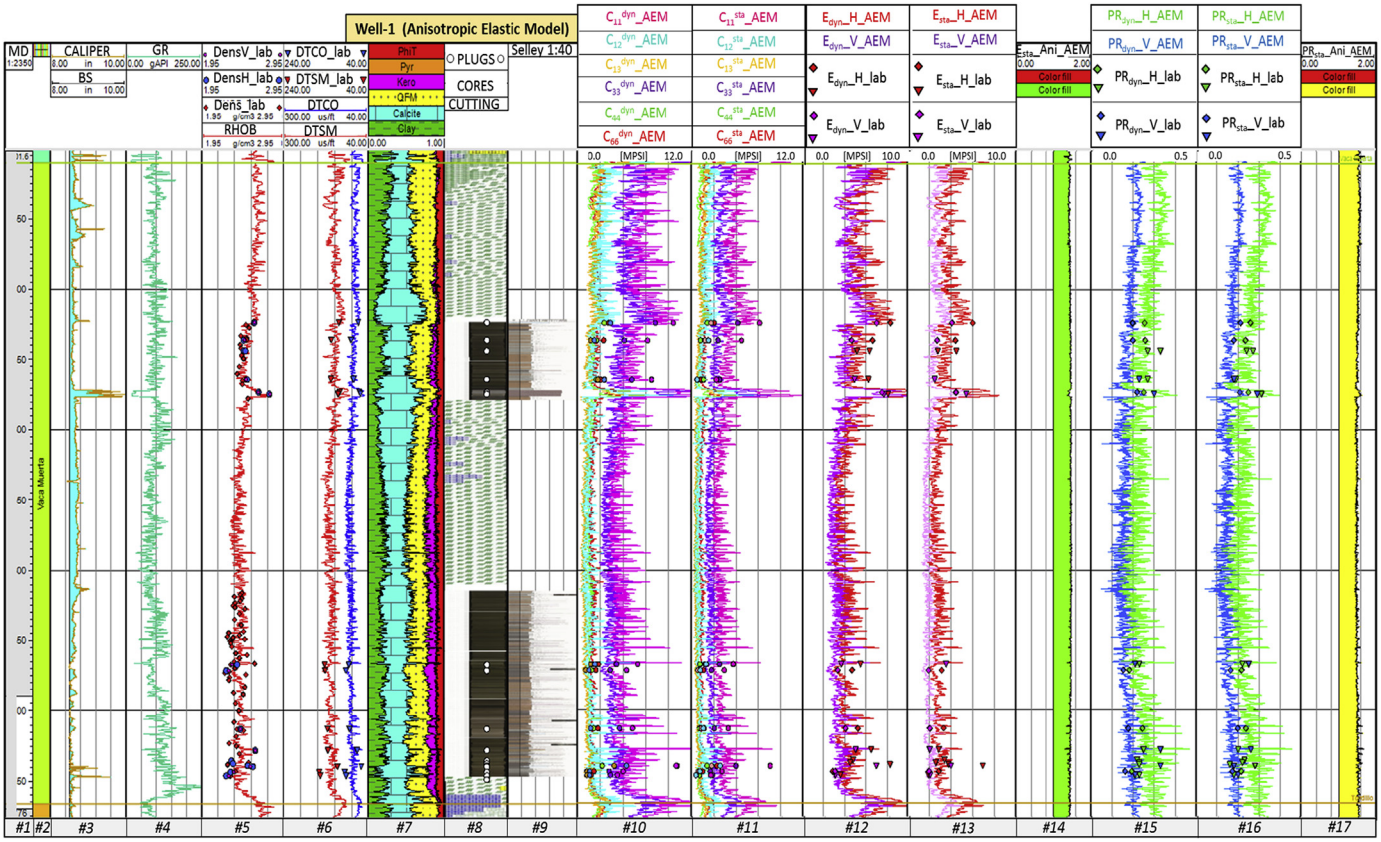

Fig. 11. Geomechanical Anisotropic Elastic Model (AEM) for a heterogeneous rock. Dots over the curves represent the calibration points measured in laboratory for each calculated curve. ***Track #1: MD***: *Measure Depth in meters;* ***#2***: *Vaca Muerta Formation;* ***#3: CALIPER*** *and* ***BS*** *(Bit Size) in inches;* ***#4: GR***: *Gamma Ray in gAPI;* ***#5: RHOB***: *Bulk Density in g/cm^3, with red and blue dots for laboratory calibration in vertical and horizontal plug direction;* ***#6: DTCO***: *Compressional Slowness and DTSM: Shear Slowness, both in us/ft;* ***#7***: *Petrophysics from gamma ray spectroscopy tool;* ***#8: CUTTING***: *Mudlogging, and* ***CORE***: *photographic core sections;* ***#9: Selley***: *Geological interpretation log;* ***#10: $C_{\alpha\beta}^{dyn}$_AEM***: *Dynamic Stiffness Coefficients for Anisotropic Elastic Model in MPSI;* ***#11: $C_{\alpha\beta}^{sta}$_AEM***: *Static Stiffness Coefficients for Anisotropic Elastic Model in MPSI;* ***#12: E_{dyn}_H_AEM and E_{dyn}_V_AEM***: *Horizontal and Vertical Dynamic Young's Modulus for Anisotropic Elastic Model in MPSI;* ***#13: E_{sta}_H_AEM and E_{sta}_V_AEM***: *Horizontal and Vertical Static Young's Modulus for Anisotropic Elastic Model in MPSI;* ***#14: E_{sta}_Ani_AEM***: *Anisotropic relation for static Young's Modulus;* ***#15: PR_{dyn}_H_AEM and PR_{dyn}_V_AEM***: *Horizontal and Vertical Dynamic Poisson Ratio for Anisotropic Elastic Model;* *and* ***#16: PR_{sta}_H_AEM and PR_{sta}_V_AEM***: *Horizontal; Vertical Static Poisson Ratio for Anisotropic Elastic Model; and* ***#17: PR_{sta}_Ani_AEM***: *Anisotropic relation for static Poisson Ratio. (For interpretation of the references to colour in this figure legend, the reader is referred to the web version of this article.)*

$$[C_{\alpha\beta}] = \begin{bmatrix} C_{11} & C_{12} & C_{13} & 0 & 0 & 0 \\ 0 & C_{11} & C_{13} & 0 & 0 & 0 \\ 0 & 0 & C_{33} & 0 & 0 & 0 \\ 0 & 0 & 0 & C_{44} & 0 & 0 \\ 0 & 0 & 0 & 0 & C_{44} & 0 \\ 0 & 0 & 0 & 0 & 0 & C_{66} \end{bmatrix}$$

C_{33}^{dyn} and C_{44}^{dyn} can be calculated as shown in Equations 10 and 11 — "From sonic log"

$$C_{11}^{dyn} = 1.27 C_{33}^{dyn} \quad \text{Equation 16}$$

$$C_{66}^{dyn} = 1.23 C_{44}^{dyn} \quad \text{Equation 17}$$

$$C_{12}^{dyn} = C_{11}^{dyn} - 2C_{66}^{dyn} \quad \text{Equation 18}$$

$$C_{13}^{dyn} = 0.76 C_{12}^{dyn} \quad \text{Equation 19}$$

"From core testing correlation"

Fig. 10 is showing the relationship between dynamic and static stiffness. The static properties were calculated based on direct measurements of Young's modulus and Poisson ratio in the lab, under static conditions, on horizontal and vertical plugs. Equations (20)–(25) are describing the relationship between Young's modulus and Poisson ratio and the obtained static stiffness tensor.

$C_{\alpha\beta}$ static properties

$$C_{11}^{sta} = \frac{E_h^{sta}\left(1 - \frac{E_h^{sta}}{E_v^{sta}} v_v^{sta^2}\right)}{\left(1 + v_h^{sta}\right)\left(1 - 2\frac{E_h^{sta}}{E_v^{sta}} v_v^{sta^2} - v_h^{sta}\right)} \tag{20}$$

$$C_{12}^{sta} = C_{11}^{sta} - 2C_{66}^{sta} \tag{21}$$

$$C_{13}^{sta} = \frac{E_h^{sta} v_v (v_h + 1)}{\left(1 + v_h^{sta}\right)\left(1 - 2\frac{E_h^{sta}}{E_v^{sta}} v_v^{sta^2} - v_h^{sta}\right)} \tag{22}$$

$$C_{33}^{sta} = \frac{E_v\left(1 - v_h^2\right)}{\left(1 + v_h^{sta}\right)\left(1 - 2\frac{E_h^{sta}}{E_v^{sta}} v_v^{sta^2} - v_h^{sta}\right)} \tag{23}$$

$$C_{44}^{sta} = \frac{E_v}{2\left(1 + v_v^{sta}\right)} \tag{24}$$

$$C_{66}^{sta} = \frac{E_h^{sta}}{2\left(1 + v_h^{sta}\right)} \tag{25}$$

where E_v^{sta}, E_h^{sta}, v_v^{sta} and v_h^{sta}, are the static elastic properties at vertical (V) and horizontal (H) directions, being E the Young's modulus (in PSI) and v the Poisson ratio.

Finally, dynamic to static correlations are applied for every $C_{\alpha\beta}$ based on correlation described in Fig. 10. The obtained anisotropic mechanical properties are used then for the whole Vaca Muerta section:

$C_{\alpha\beta}$ dynamic to static correlations

In the AEM (Fig. 11), tracks 1 to 9 are the same as in Fig. 8. Equations (9)–(25) (linear elastic assumptions, dynamic correlations from laboratory and dynamic to static correlations) were applied to obtain the $C_{\alpha\beta}^{dyn}$ and $C_{\alpha\beta}^{sta}$. Those properties were used to calculate E_V, E_H, v_v and v_h, the elastic properties at vertical (V) and horizontal (H) directions, for both, dynamic and static conditions, with E the Young's modulus and v the Poisson ratio in equations (26)–(29).

$$E_H = \frac{(C_{11} - C_{12})(C_{11}C_{33} - 2C_{13}C_{13} + C_{12}C_{33})}{C_{11}C_{33} - C_{13}C_{13}} \tag{26}$$

$$E_V = C_{33} - \left[\frac{2C_{13}C_{13}}{C_{11} + C_{12}}\right] \tag{27}$$

$$PR_H = \frac{C_{13}}{C_{11} + C_{12}} \tag{28}$$

$$PR_V = \frac{C_{33}C_{12} - C_{13}C_{13}}{C_{11}C_{33} + C_{13}C_{13}} \tag{29}$$

Stiffness curves highly correlate with their laboratory measurements (Fig. 11, tracks 10 and 11). Tracks 12 and 13 show

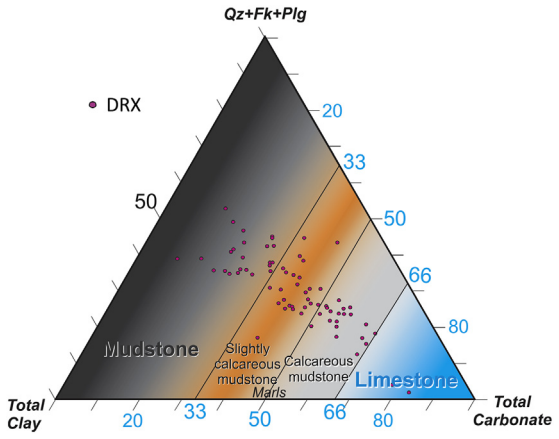

Fig. 12. Classification scheme for organic mudstones based on bulk mineralogy. Note the marl subclassification proposed for the mechanical stratigraphy. Modified and simplified from Gamero-Díaz et al. (2012).

dynamic and static Young's modulus respectively, where dynamic properties are higher than static, and the horizontal properties show greater stiffness than the vertical ones, mainly due to the laminated nature of this type of rocks. Calibration with laboratory tests shows a stiffer behavior in core samples than the calculated curves for static and dynamics properties, probably a a result of differences in frequency measurements from well log and laboratory. Track 14 shows Young's anisotropy, defined as the relationship between E_h and E_v, along Vaca Muerta Formation. Anisotropy is reduced in upper Vaca Muerta (40%), when comparing to middle (45%) and lower Vaca Muerta (40%). More carbonate rich layers and volcanic sills, alternating into the sequence, have low anisotropy, reaching 25%. Tracks 15 and 16 show dynamic and static Poisson ratio respectively, where it is possible to observe a similar trend for the Young's modulus, with horizontal properties higher than verticals. Track 17 show Poisson's ratio anisotropy along Vaca Muerta Formation, and is suggesting anisotropy ranging on about 50–55% at the top and base, and 45–50% for the middle section.

3.1.3. *Detailed Anisotropic Elastic Model (DAEM)*

The Vaca Muerta Formation displays different lithologies. Quartz-feldespar-mica, carbonate, clays (mainly illite, caolinite and less smectite), kerogen and pyrite. They were all used to perform the petrophysical classification. The methodology for creating a detailed mineralogy-based description for organic mudstones using core and geochemical log data is based upon Gamero-Díaz et al.

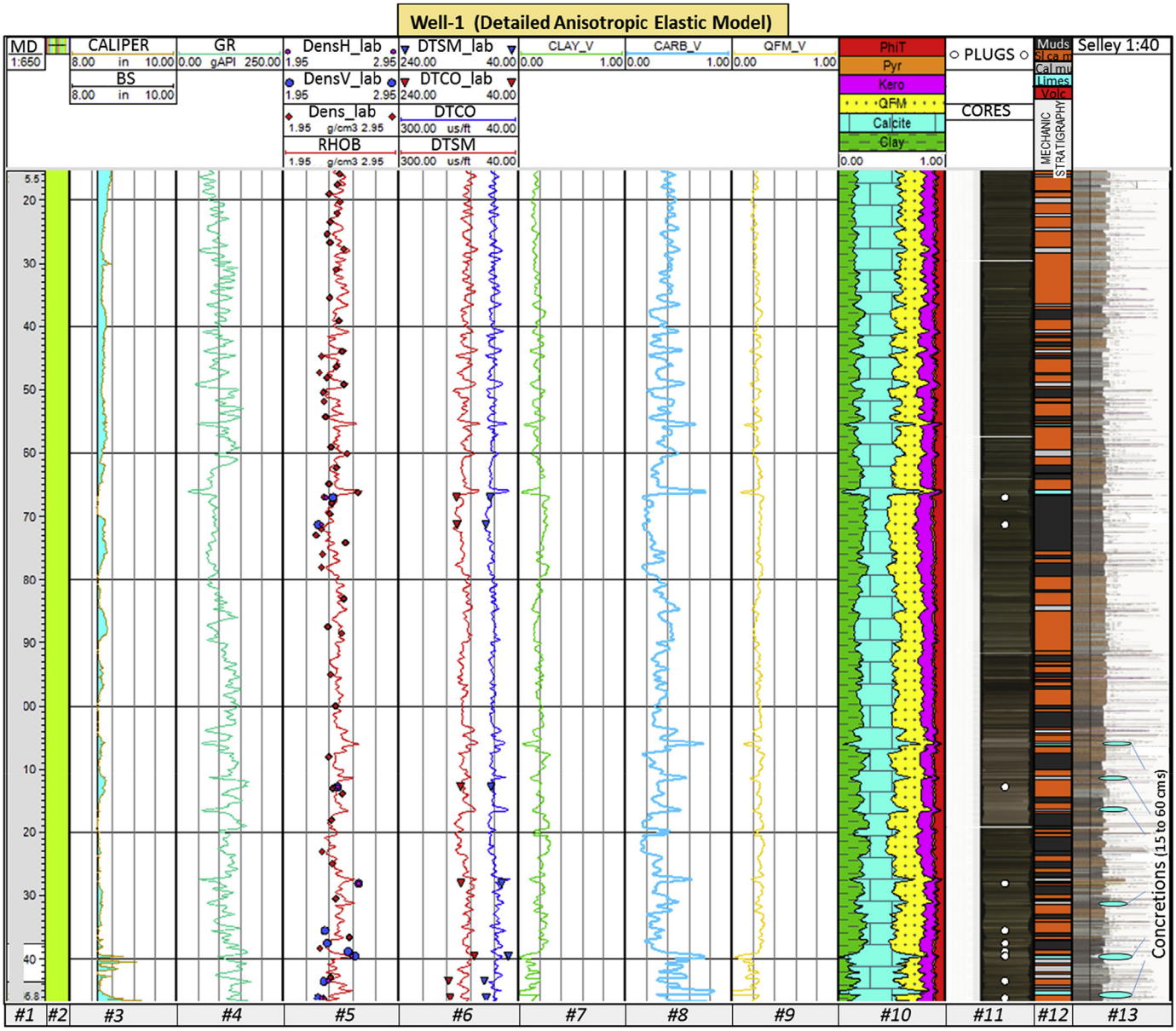

Fig. 13. Input data curves for DAEM, showing the match between the mechanic stratigraphy and Selley log for the Vaca Muerta Formation base. ***Track #1: MD****: Measure Depth in meters;* ***#2****: Vaca Muerta Formation;* ***#3: CALIPER*** *and* ***BS*** *(Bit Size) in inches;* ***#4: GR****: Gamma Ray in gAPI;* ***#5: RHOB****: Bulk Density in g/cm^3, with red and blue dots for laboratory calibration in vertical and horizontal plug direction;* ***#6: DTCO****: Compressional Slowness and DTSM: Shear Slowness, both in us/ft;* ***#7: CLAY_V****: Total Clay Volume;* ***#8: CARB_V****: Total Carbonate Volume;* ***#9: QFM_V****: Quartz-Feldspar-Mica Volume;* ***#10****: Petrophysics from gamma ray spectroscopy tool;* ***#11: CORE****: photographic core sections;* ***#12: MECHANIC STRATIGRAPHY*** *(with Muds=Mudstone, Sl_ca_m=Slightly calcareous mudstone, Cal_mu=Calcareous mudstone, Limes=Limestone and Volc=Volcanic layers); and* ***#13: Selley****: Geological interpretation log. (For interpretation of the references to colour in this figure legend, the reader is referred to the web version of this article.)*

(2012) (Fig. 12). A series of cut-off values for the petrophysical carbonate content (track number 8 in Fig. 13) have been applied for lithological facies simplification. It allows performing a mechanical stratigraphy that matches with the Selley log (tracks 11 and 13 in Fig. 13), where the main lithological facies are mudstone, slightly calcareous mudstone, calcareous mudstone and limestone (based on the lithological core description).

The rock set displayed in the mechanical stratigraphy presents a variety of elastic to inelastic and stress sensitive behaviors.

The mathematical workflow for DAEM follows the same procedure shown in equations (9)–(29). For this model, it is even more recommended to have a large number of samples considering that the reduction made by the facies discrimination is important.

The main difference is that each facies groups have its own correlation (Fig. 14), differentiated by its carbonate content. Mudstones and slightly calcareous mudstone (black and orange dots respectively), present low calcite content, while the calcareous mudstone and limestones (grey and blue dots respectively) hold more calcite. The slope of the correlations varies from blue, grey, orange and black, getting steeper and steeper, suggesting that they have different behaviors. The change in the slope is considered to be directly associated with the anisotropy of the rock, with increasing in the anisotropic behavior from limestone to mudstone. Linear trend parallel and close to the 1:1 line, means that those rocks are more similar between their symmetry axes, like isotropic rocks. These results are consistent with data published by Suarez-Rivera et al. (2011). In addition, the black, orange and grey dots show more compliant behavior than the blue dots, which also are stiffer than the rest.

Similarly, to the previous two models, this detailed anisotropic model presents dynamic properties higher than static properties (Fig. 15), where lithological facies describe distinct mechanical behavior. The trending is not so clear between facies, where at least it is possible to observe a certain tendency among the mudstones, slightly calcareous mudstones and calcareous mudstones, to show much more difference in between dynamic and static properties in that order, while limestones show random behavior. This latter may be due to the correlation performed with two samples that display high stiffness parameters.

Fig. 16 shows the geomechanical DAEM for the whole Vaca Muerta Formation at Well-1. The necessary input data for calculating an elastic model are shown in tracks 3 to 10. Each group of facies represented in the mechanical stratigraphy (track 9), displays different correlations, as it was shown in Figs. 14 and 15.

From tracks 11 and 12 it is possible to observe that stiffness curves correlate well with their laboratory measurements (almost in the same range), but due to the different correlations used for lithologies, curves are spikier, giving more contrast between those lithology groups. Tracks 13 and 14 show respectively, dynamic and static Young's modulus. Young's modulus at horizontal direction is higher than that of the vertical direction (around 60%), being quite similar to the calcareous sections and volcanic sills, which show

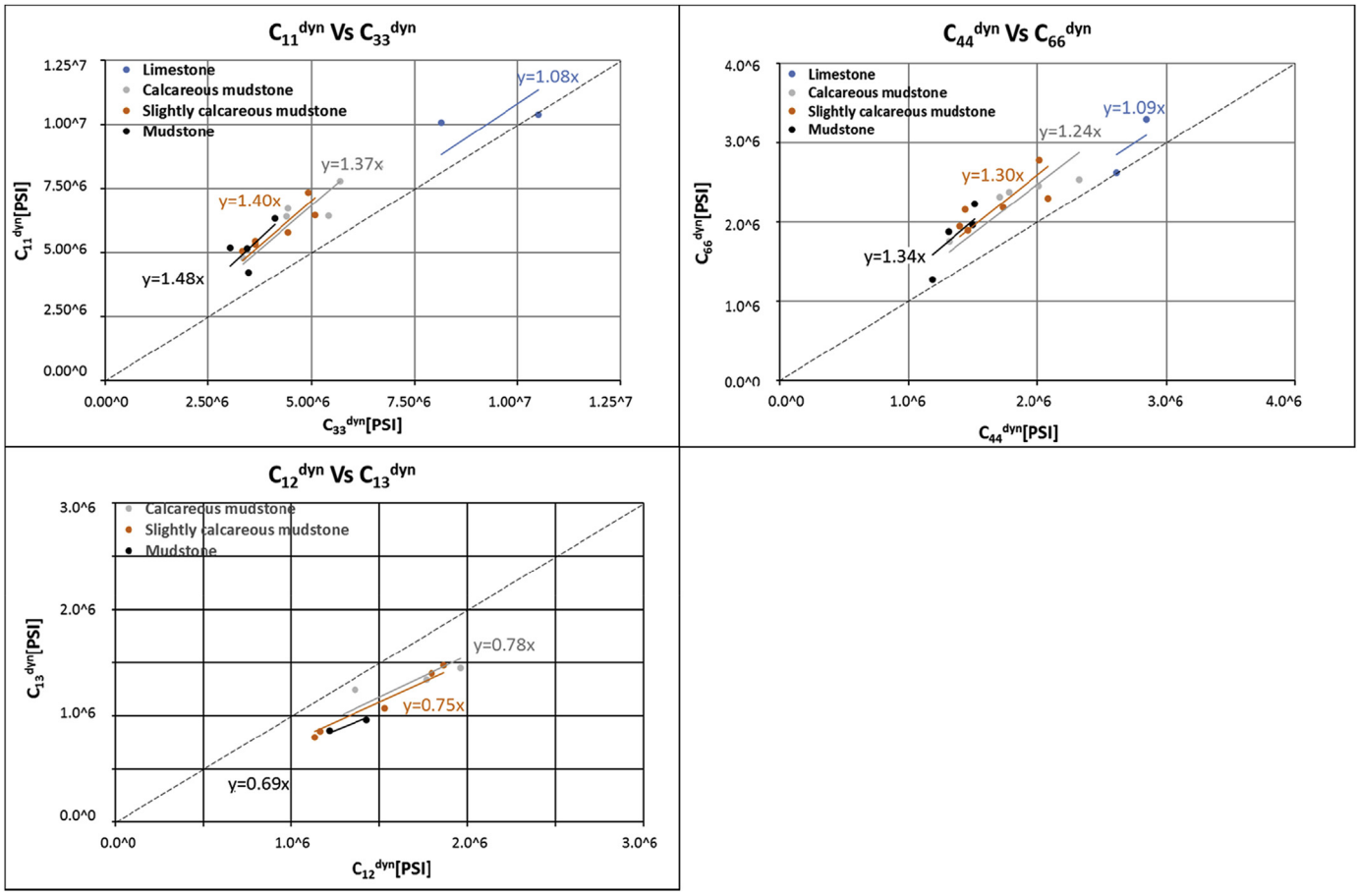

Fig. 14. C_{11d}, C_{13d}, C_{33d}, C_{44d} and C_{66d}, are the five independent elastic stiffness coefficients that characterize a transversely isotropic material. Correlations represent the amount of anisotropy between vertical and horizontal directions for different lithologies, being the blue dots limestones, grey dots calcareous mudstones, orange dots slightly calcareous mudstones and black dots mudstones. Note the anisotropy increasing behavior, with the reduction in calcite concentration. (For interpretation of the references to colour in this figure legend, the reader is referred to the web version of this article.)

less anisotropy (around 15%–20%, tracks 15 and 16). Calibration with laboratory tests seems to fit better in static properties than dynamic (same phenomena is observed in Fig. 11). Tracks 17 and 18 show respectively, dynamic and static Poisson ratio, with their calibration points, in good agreement. Dynamic and static tendencies correlate as expected, where it is possible to observe dynamic parameters higher than static. Horizontal properties are higher than vertical across the Vaca Muerta Formation.

During the dynamic to static correlation analysis by lithofacies some discrepancies have been found. The anisotropies found in laboratory in each lithology, could not be represented in Young's modulus and Poisson ratio anisotropies (tracks 15 y 16). In addition, for Poisson ratio anisotropy, it is possible to observe a curve with wicked quality and too spiky, that barely represents the real rock. The main hypothesis to explain this latter unpredictable behavior could be the lack of data points, with many erratic static values, that led to perform calibration based on poor statistic. Due to the issues described above, an extra model was established for the DAEM, call DAEM2, where the dynamic to static correlation has been carried on using the general correlation for Vaca Muerta Formation applied in the AEM (as an average from all the lithologies). The resulting curves (tracks 16 and 20), proved to reproduce the behavior observed in laboratory. Thus the anisotropy varies according to the calcite content, resulting mudstones and slightly calcareous mudstones to be much anisotropic (Young's 55%–70% and Poisson 50%–70%) and, on the other hand, the calcareous mudstones and limestones resulted to be less anisotropic rocks (Young's 20%–55% and Poisson around 50%).

4. Discussion: comparison between models

To obtain a representative in-situ stress model with its fracture gradient (Fig. 17), it is mandatory first to have an excellent knowledge of the elastic model around the wellbore. Nowadays, there is no agreement within the scientific community about what type of elastic model should be used, how much detail it should have and how much time it demands to be build. One of the reasons why most shale plays apply for an isotropic simplification is related to limitations when measuring the dynamic elastic constants (Mavko and Bandyopadhyay, 2009).

In this work, it is concluded that the degree of representativeness will depend upon the application purpose, depending on what is being modeled and the scope of that model.

An IEM will be useful for extended homogeneous rock masses with weak anisotropy (e.g. eolian sandstone, located in basins with poor tectonics). There is no need to perform anisotropic laboratory

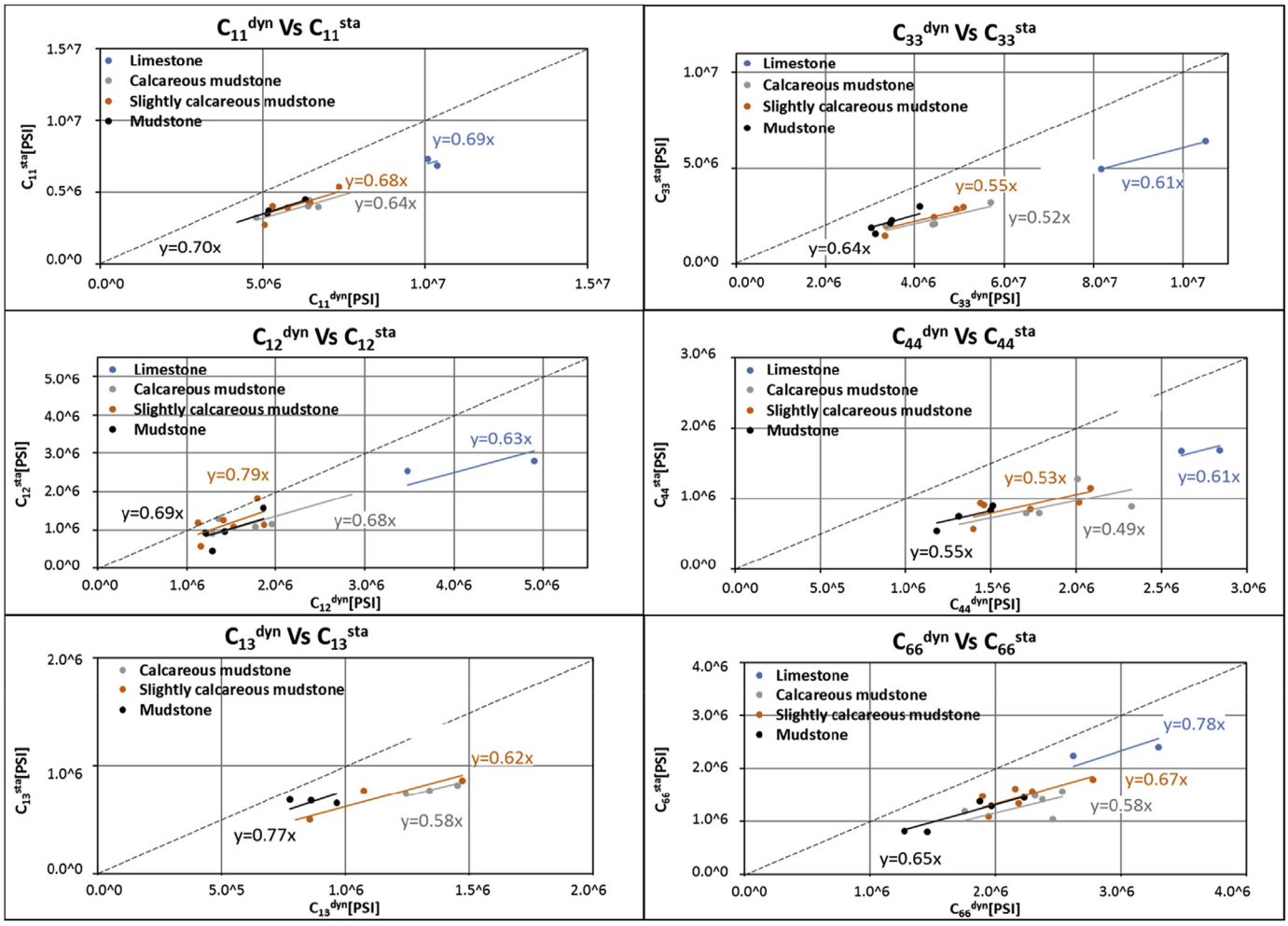

Fig. 15. Dynamic to Static Stiffness correlations for C_{11}, C_{12}, C_{13}, C_{33}, C_{44} and C_{66}. The correlations are represented by linear regressions (with interception in "0"). Blue dots represents limestones, grey dots calcareous mudstones, orange dots slightly calcareous mudstones and black dots mudstones. Slightly calcareous mudstones and mudstones represents the less calcareous and laminated rocks. (For interpretation of the references to colour in this figure legend, the reader is referred to the web version of this article.)

tests, the use of sophisticated log tools and advanced modeling. The practical use of an isotropic elastic model in heterogeneous rocks like Vaca Muerta Formation can be only justified for quick view, identifying elastic properties and their limits. This practice is not recommended because of the minimum horizontal stress "σ_h" underestimation, as suggested in this work (see Fig. 17, track 9), and proved by other authors like Hamza et al. (2015). It is important to mention that horizontal stresses have been calculated using "σ_v" (vertical stress) calculated from density log, "Pp" (pore pressure) assuming a constant gradient matching with overpressure events as gas influx, mud weight, MDT, etc., Biot coefficient calculated from K_b and K_g (bulk modulus and bulk grain respectively) for isotropic model and $C^{sta}_{\alpha\beta}$ for anisotropic model, finally, tectonic minimum strain have been calibrated with the purpose to match the "σ_h" horizontal minimum stress with the ISIP (instantaneous shut in pressure) in four wells in the area, and the tectonic maximum strain have been calibrated in relation to obtain a strike slip to normal regime in the area, where the "σ_H" horizontal maximum stress will be from equal to higher than "σ_v".

Current works identify anisotropy in the order of magnitude between an average of 40%–45% for Young's modulus (E_H/E_V) in an AEM and 20%–70% for a DAEM2 (Fig. 18). It is extremely important to note, that for vertical wells, the isotropic models will represent only vertical properties, because of the way that the log tool works in the hole, and the equations used. In Fig. 17, it is clear that isotropic Young's modulus (black dashed curve) overlaps the vertical anisotropic Young's modulus (pink curve) and the detailed vertical anisotropic Young's modulus (violet curve). But, this relation is not that clear in isotropic Poisson ratio (black dashed curve), which seems to be an average between vertical and horizontal anisotropic properties. On the other hand, a DAEM will be the most realistic model to be applied in heterogeneous rocks (even with anisotropic stresses). Large amount of data is required to model each facies group, processing many correlations. Triaxial laboratory tests will be needed (testing rocks at vertical, horizontal and 45° directions). Sophisticated log tools with different sonic waves measurements (shear, compressional and Stoneley) will be also required. Advanced mathematical expressions, like a four rank tensor matrix, will be needed. Finally, this workflow demands a large amount of time and requires a multidisciplinary team to deal with different technical areas. A simple AEM with the main assumption that every rock lithotype will be elastic and following the same transforms seems to be the more efficient model. It does not require facies discrimination, is easy to process, requires less

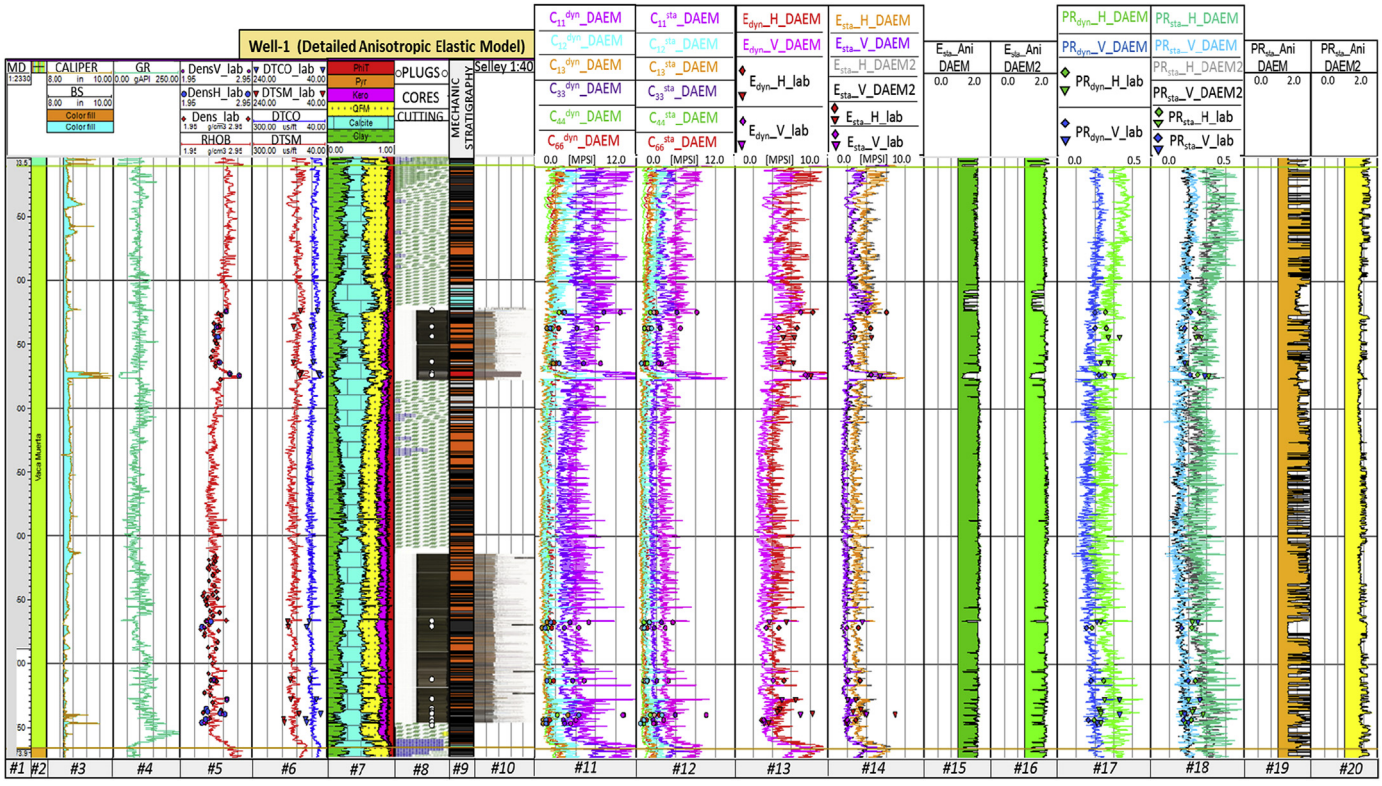

Fig. 16. Geomechanical Detailed Anisotropic Elastic Model (DAEM) for a heterogeneous rock. Dots over the curves represents the calibration points measured in laboratory for each calculated curve. ***Track #1: MD***: *Measure Depth in meters;* ***#2***: *Vaca Muerta Formation;* ***#3: CALIPER*** *and* ***BS*** *(Bit Size) in inches;* ***#4: GR***: *Gamma Ray in gAPI;* ***#5: RHOB***: *Bulk Density in g/cm^3, with red and blue dots for laboratory calibration in vertical and horizontal plug direction;* ***#6: DTCO***: *Compressional Slowness and DTSM: Shear Slowness, both in us/ft;* ***#7***: *Petrophysics from gamma ray spectroscopy tool;* ***#8: CUTTING***: *Mudlogging, and* ***CORE***: *photographic core sections;* ***#9: MECHANIC STRATIGRAPHY***; ***#10: Selley***: *Geological interpretation log;* ***#11: $C^{dyn}_{\alpha\beta}$_DAEM***: *Dynamic Stiffness Coefficients for Detailed Anisotropic Elastic Model in MPSI;* ***#12: $C^{sta}_{\alpha\beta}$_DAEM***: *Static Stiffness Coefficients for Detailed Anisotropic Elastic Model in MPSI;* ***#13: E_{dyn}_H_DAEM and E_{dyn}_V_DAEM***: *Horizontal and Vertical Dynamic Young's Modulus for Detailed Anisotropic Elastic Model in MPSI;* ***#14: E_{sta}_H_DAEM & E_{sta}_H_DAEM2 and E_{sta}_V_DAEM & E_{sta}_V_DAEM2***: *Horizontal and Vertical Static Young's Modulus for Detailed Anisotropic Elastic Model in MPSI;* ***#15: E_{sta}_Ani_DAEM***: *Anisotropic relation for static Young's Modulus;* ***#16: E_{sta}_Ani_DAEM2***: *Anisotropic relation for static Young's Modulus (calculated without lithology discrimination);* ***#17: PR_{dyn}_H_DAEM and PR_{dyn}_V_DAEM***: *Horizontal and Vertical Dynamic Poisson Ratio for Detailed Anisotropic Elastic Model;* ***#18: PR_{sta}_H_DAEM & PR_{sta}_H_DAEM2 and PR_{sta}_V_DAEM & PR_{sta}_V_DAEM2***: *Horizontal; Vertical Static Poisson Ratio for Detailed Anisotropic Elastic Model; and* ***#19: PR_{sta}_Ani_DAEM***: *Anisotropic relation for static Poisson Ratio; and* ***#20: PR_{sta}_Ani_DAEM2***: *Anisotropic relation for static Poisson Ratio (calculated without lithology discrimination). (For interpretation of the references to colour in this figure legend, the reader is referred to the web version of this article.)*

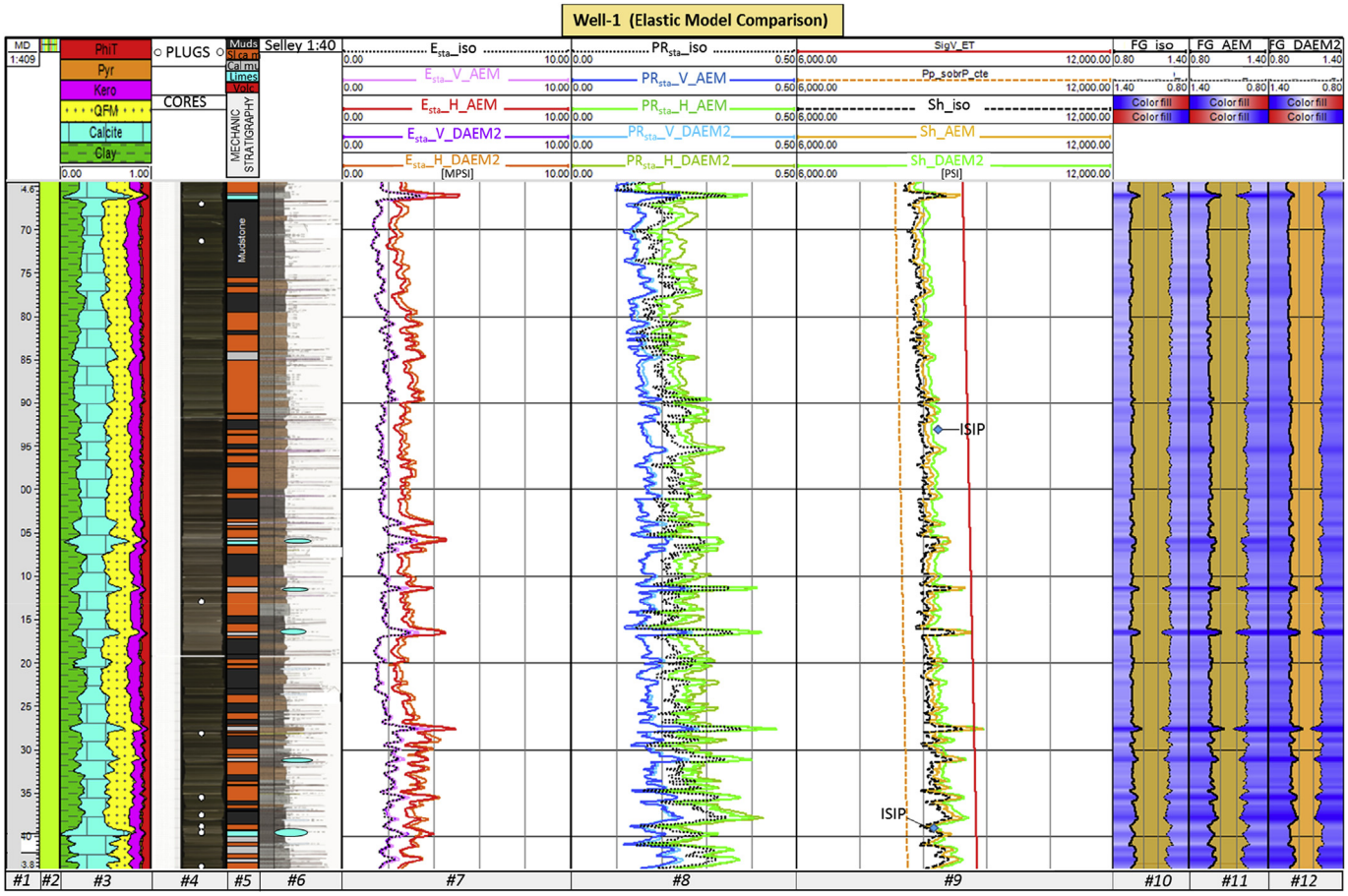

Fig. 17. Elastic model comparison with field calibration points for the minimum horizontal stress and Fracture Gradient. ***Track #1: MD***: *Measure Depth in meters;* ***#2***: *Vaca Muerta Formation;* ***#3***: *Petrophysics from gamma ray spectroscopy tool;* ***#4: CUTTING***: *Mudlogging, and* ***CORE***: *photographic core sections;* ***#5: MECHANIC STRATIGRAPHY***; ***#6: Selley***: *Geological interpretation log;* ***#7: E_{sta}_iso***: *Static Isotropic Young Modulus,* ***E_{sta}_H_AEM and E_{sta}_V_AEM***: *Horizontal and Vertical Static Young's Modulus for Anisotropic Elastic Model,* ***E_{sta}_H_DAEM and E_{sta}_V_DAEM***: *Horizontal and Vertical Static Young's Modulus for Detailed Anisotropic Elastic Model in MPSI;* ***#8: PR_{sta}_iso***: *Static Isotropic Poisson Ratio,* ***PR_{sta}_H_AEM and PR_{sta}_V_AEM***: *Horizontal and Vertical Static Poisson Ratio for Anisotropic Elastic Model,* ***PR_{sta}_H_DAEM and PR_{sta}_V_DAEM***: *Horizontal; Vertical Static Poisson Ratio for Detailed Anisotropic Elastic Model;* ***#9: SigV_ET***: *Vertical Stress,* ***Pp_SobrP_cte***: *Pore Pressure Constant (calibrated with inflows, kicks, mud weight, etc),* ***Sh_iso***: *Isotropic Minimum Horizontal Stress,* ***Sh_AEM***: *Anisotropic Minimum Horizontal Stress (calibrated with ISIP=Instantaneous Shut in Pressure, LOT=Leak Off Test, MFO=Mini Fall Off, etc),* ***Sh_DAEM***: *Anisotropic "Detailed" Minimum Horizontal Stress in PSI;* ***#10: FG_iso***: *Isotropic Fracture Gradient;* ***#11: FG_AEM***: *Anisotropic Fracture Gradient;* ***#12: FG_DAEM***: *Detailed Anisotropic Fracture Gradient.*

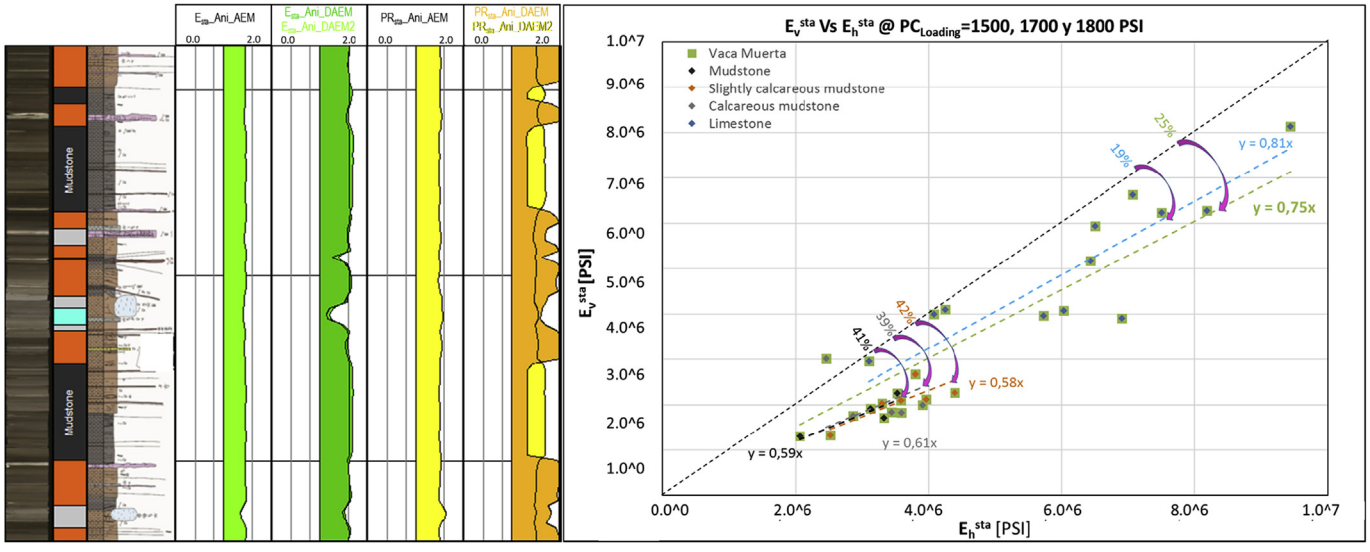

Fig. 18. Crossplot for static Young's modulus anisotropical evaluation, performed in laboratory with facies discrimination and the continuous logs for the entire Vaca Muerta Formation. Observe better anisotropy agreement in average with the AEM, but better definition in contrast behaviors with the DAEM2.

laboratory measurements than a DAEM (earning time), and requires fewer interpretations to be applied for any geological environment.

Finally, three fracture gradients curves (FG) have been calculated (each one corresponding to a different elastic model). As it was mentioned before, the isotropic model underestimates the minimum horizontal stress. This latter clearly impacts in the FG, where the IEM presents lower gradients than the AEM, and the AEM presents lower gradients than the DAEM. It is also interesting to note the relation between FG peaks with high calcite content rocks and volcanic sills, leading to detect barriers for hydraulic fracture growth between contrasting rock mechanical behaviors, and the occurrence of "T" shape fractures in depth (as analogues to outcrops Fig. 3d).

5. Conclusions

Vaca Muerta Formation presents high heterogeneity, represented by horizontal and vertical variations in lithology. Also, the horizontal and vertical stresses vary with depth and orientation. Those phenomenon leads to an anisotropic stress field, requiring different geomechanical elastic model to be analyzed. The Isotropic Elastic Model represents the easiest model, but this simplicity makes it vulnerable for a rigorous analysis and leads to poor applications in the oil industry (e.g. hydraulic fracturing).

A better model will be the Elastic Anisotropic Model, with a VTI anisotropic model. Enough data and mathematical simplicity make it efficient to perform an anisotropic stress model, where differences with results obtained by the isotropic model would be huge and differences with a detailed model would be minor.

If there is much more information available like the number of wells, full core for many of them, high resolution and complete well log sets, geological core description, triaxial laboratory test, seismic, perforation events, well interventions, etc., the recommended practices will be to integrate all this data, and perform a Detailed Anisotropic Elastic Model. This model will apply for specifics fields, representing improvements in elastic anisotropic analysis in different lithologies, allowing estimating better regional stresses, greater efficiency in detecting fracture barriers, etcetera. This task will lead to truly improvements at the time to run unconventional well completion (well placement, well orientation, landing, perforating, hydraulic fracturing, production, etcetera).

Acknowledgments

The authors thank Chevron Argentina and International for financing, providing essential data and well plugs, and for the permission to publish this paper. Instituto Tecnológico de Buenos Aires to intermediate and provide the possibility to get samples in Neuquén Basin and finance the work trip to UT Austin. The University of Texas at Austin for financing and providing the specific equipment and especially thanks to Matthew Ramos for the laboratory assistance to carry out this work. Finally, Schlumberger Argentina for providing specialized software and technical support.

References

Amadei, B., 1996. Importance of anisotropy when estimating and measuring in situ stress in rock. Int. J. Rock Mech. Min. Sci. Geomech. Abstr 33 (No. 3).

Askenazi, A., Biscayart, P., Cáneva, M., Montenegro, S., Moreno, M., 2013. Analogía entre la Formación Vaca Muerta y Shale Gas/Oil Plays de EEUU. YPF S.A. Copyright 2013. Society of Petroleum Engineers.

Barredo, S.P., Stinco, L.P., 2013. A geodynamic view of oil and gas resources associated to the unconventional shale reservoirs of Argentina. In: Paper URTEC 1593090 Presented and Published by Unconventional Resources Technology Conference, 10pps.

Barree, R.D., Gilbert, J.V., 2009. Stress and rock property profiling for unconventional reservoir stimulation. In: SPE Hydraulic Fracturing Technology Conference Held in the Woodlands. Texas, USA, 19–21 January 2009. Paper N°: SPE 118703.

Belikov, B.A., 1970. Elastic Properties of Rock Minerals and Rocks. Nauka, Moscow.

Canady, W., 2010. A method for full-range Young's modulus correction. In: Presented at the SPE North American Unconventional Gas Conference and Exhibition. The Woodlands, Texas, USA, 14–16 June. SPE-143604-MS.

Chertov, M., 2012. Closed-form solution for vertical fracture width in anisotropic elastic formations. Int. J. Rock Mech. Min. Sci. 53, 70–75.

Cuervo, S., Dolores Vallejo, M., Crousse, L., 2014. Integrated petrophysical and geomechanical characterization of the Vaca Muerta Formation in El trapial area. In: IX Congreso de Exploración y Desarrollo de Hidrocarburos Simposio de Recursos No Convencionales: Ampliando el Horizonte Energético.

Eissa, E.A., 1988. Relation between static and dynamic Young's modulus of rocks. Int. J. Rock Mech. 25, 479–482.

Energy Information Administration, 2014. Country Analysis Note. United State. http://www.eia.gov/todayinenergy/detail.php?id=14431.

Fantin, M., Crousse, L., Cuervo, S., Vallejo, D., González Tomassini, F., Reijenstein, H., Lipinski, C., 2014. Vaca Muerta stratigraphy in central Neuquén basin: impact on emergent unconventional project. In: Unconventional Resources Technology Conference (URTeC). http://dx.doi.org/10.15530/urtec-2014-1923793. Denver Colorado, USA.

Fjaer, E., Holt, R., Horsrud, P., Raaen, A., Risnes, R., 2008. Petroleum Related Rock Mechanics, second ed., p. 41

Frydman, M., Pacheco, F., Pastor, J., Canesin, F., Caniggia, J., Davey, H., 2016. Comprehensive determination of the far-field earth stresses for rocks with anisotropy in tectonic environment. In: SPE Argentina Exploration and Production of Unconventional Resources Symposium Held in Buenos Aires, Argentina, 1–3 June 2016. SPE-SPE-180965-MS-MS.

Gamero-Díaz, H., Miller, C., Lewis, R., 2012. sCore: a Classification Scheme for Organic Mudstones Based on Bulk Mineralogy. Search and Discovery Article #40951.

Gorjainov, N.L., 1979. Seismic Methods in Engineering Geology. Nedra, Moscow.

Gulisano, C.A., Gutiérrez Pleimling, A.R., Digregorio, R.E., 1984. Esquema estratigráfico de la secuencia jurásica del oeste de la provincia del Neuquén. In: IX Congreso Geológico Argentino. Actas 1, pp. 236–259. Bariloche.

Haldorsen, J.B., Johnson, D., Plona, T., Sinha, B., Valero, H., Winkler, K., 2006. Acústica de Pozo. Summer 2006 Oilfield Rev. 36–45. Ridgefield, Connecticut, EUA.

Hamza, F., Chen, C., Gu, M., Quirein, J., Martysevich, V., Matzar, L., 2015. Characterization of anisotropic elastic moduli and stress for unconventional reservoirs using laboratory static and dynamic geomechanical data. In: SPER/CSUR Unconventional Resources Conference Held in Calgary, Alberta, Canada, 20–22 October 2015. SPE-175907-MS.

Havens, J., 2011. Mechanical Properties of the Bakken Formation. M.Sc. Thesis. Colorado School of Mines, Golden, USA.

Kietzmann, D.A., Palma y, R.M., Bressan, G.S., 2008. Facies y microfacies de la rampa tithoniana-berriasiana de la Cuenca Neuquina (Formación Vaca Muerta) en la sección del arroyo Loncoche – malargüe, provincia de Mendoza. Rev. la Asoc. Geol. Argent. 63 (4), 969–713.

Kuila, U., Dewhurst, D., Siggins, A., Raven, M., 2010. Stress anisotropy and velocity anisotropy in low porosity shale. Tectonophysics 503 (2011), 34–44.

Lacy, L.L., 1997. Dynamic rock mechanics testing for optimized fracture designs. In: Presented at the SPE Annual Technical Conference and Exhibition, San Antonio, Texas, USA, 5–8 October. SPE-38716-MS.

Lee, H., Ong, S., Azeemuddin, M., Goodman, H., 2012. A wellbore stability model for formations with anisotropic rock strengths. J. Petroleum Sci. Eng. 96–97, 109–119.

Legarreta, L., Gulisano, C., 1989. Análisis estratigráfico de la Cuenca Neuquina (Triásico Superior-Terciario Inferior). In: Chebli, G., Spalletti, L. (Eds.), Cuencas Sedimentarias Argentinas. Simposio Cuencas Sedimentarias Argentinas, vol. 6. Universidad de Tucumán, Serie Correlación Geológica, Tucumán, pp. 221–243.

Legarreta, L., Gulisano, C.A., Uliana, M.A., 1993. Las secuencias sedimentarias jurásicas-cretácicas. Mendoza 1(9). In: Relatorio Geología y Recursos Minerales de Mendoza. XII Congreso Geológico Argentino y II Congreso de Exploración de Hidrocarburos, pp. 87–114.

Legarreta, L., Villar, H., 2011. Geological and Geochemical Keys of the Potential Shale Resources, Argentina Basins. Search and Discovery Article #80196 (2011).

Marlats, A., Tórtora, L., 2014. Sedimentology Study of the Vaca Muerta Formation in the El Trapial Field. Confidential report prepared from LCV to Chevron Argentina S.R.L.

Mavko, G., Bandyopadhyay, K., 2009. Approximate fluid substitution for vertical velocities in weakly anisotropic VTI rocks. Geophysics 74 (1), 2009.

Mavko, G., Mukeji, T., Dvorkin, J., 2009. The Rock Physics Handbook, second ed. Cambridge University Press, Cambridge, United Kingdom.

Mavko, G., Mukerji, T., Godfrey, N., 1995. Predicting stress-induced velocity anisotropy in rocks. Geophys 60, 1081–1087.

Maxwell, S., 2009. Microseismic location uncertainty. CSEG Rec. 34 (4), 41–46.

McCann, D.E., 1992. Determination of Young's modulus of the rock mass from geophysical logs. Geol. Soc. Lond. Spec. Publ. 65 (1), 317–325.

Mese, A., Tutuncu, A., 2011. Impact of fluids and formation anisotropy on acoustic, deformation and failure characteristics of reservoirs shales and pure clay minerals. In: ISRM 491, Proceedings of International Society of Rock Mechanics (ISRM) (Beijing, China).

Mitchum, R.M., Uliana, M.A., 1985. Seismic stratigraphy of carbonate depositional sequences, upper jurassic-lower cretaceous, neuqué basin, Argentina. In:

Bero, B.R., WoolvertoN, D.G. (Eds.), Seismic Stratigraphy: an Integrated Approach to Hydrocarbon Exploration, pp. 255–274. AAPG Memoirs 39.
Mohaghegh, S., 2013. A critical view of current state of reservoir modeling of shale assets. In: Proc. Of SPE Eastern Regional Meeting, Pittsburg, USA. SPE-165713.
Mokhtari, M., Alqahtani, A., Tutuncu, A., 2013a. Failure behavior of anisotropic shales. In: ARMA 13–312, Proc. Of the 47th US Rock Mechanics/Geomechanics Symposium, San Francisco, USA.
Mokhtari, M., Alqahtani, A., Tutuncu, A., Yin, X., 2013b. Stress-dependent permeability anisotropy and wettability of shale resources. In: Proc. Of the 1st Unconventional Resources Technology Conference. Denver, USA. SPE-168672.
Mokhtari, M., Honarpour, M., Tutuncu, A., Boitnott, G., 2014a. Acoustical and geomechanical characterization of Eagle Ford shale – anisotropy, heterogeneity and measurement scale. In: SPE Annual Technical Conference and Exhibition. Amsterdam, the Netherlands, 27–29 October 2014. SPE-170707-MS.
Mokhtari, M., Tutuncu, A., Kazemi, H., 2014b. Integrated study on tensile fracture mechanics and subsequent flow in naturally-fractured Niobara shale. In: ARMA 14–7126, Proc. Of the 48th US Rock Mechanics/Geomechanics Symposium, Minneapolis, USA.
Morales, R.H., Marcinew, R.P., 1993. Fracturing of high-permeability formations: mechanical properties correlations. In: Presented at the SPE Annual Technical Conference and Exhibition, Houston, Texas, USA, 3–6 October. SPE-26561-MS.
Nur, A., Simmons, G., 1969. Stress induced velocity anisotropy in rock: an experimental study. J. Geophys. Res. 74, 6667–6674.
Radovitzky, R., 2003. Técnicas de análisis y diseño estructural. MIT Open Course Ware, Maschusetts Institute of Technology. http://mit.ocw.universia.net/16.21/OcwWeb/Aeronautics-and-Astronautics/16–21Techniques-of-Structural-Analysis-and-DesignSpring.2003/CourseHome/index.htm.
Rodrigues, N., Cobbold, P.R., Loseth, H., Ruffet, G., 2009. Widespread bedding-parallel veins of fibrous calcite ("beef") in a mature source rock (Vaca Muerta Fm, Neuquén Basin, Argentina): evidence for overpressure and horizontal compression. J. Geol. Soc. Lond. 166 (4), 695–709. http://dx.doi.org/10.1144/0016-76492008-111.
Rüger, A., 1996. Reflection Coefficients and Azimuthal AVO Analysis in Anisotropic Media. Doctoral Thesis. Center for Wave Phenomena, Colorado School of Mines.
Scasso, R.A., Alonso, M.S., Lanés, S., Villar, H.J., Lippai, H., 2002. Petrología y geoquímica de una ritmita marga-caliza del Hemisferio Austral: El Miembro Los Catutos (Formación Vaca Muerta), Tithoniano medio de la Cuenca Neuquina. Rev. Asoc. Geol. Argent. 57 (2), 143–159.
Serejian, V., Ghassemi, A., 2011. Hydraulic fracture initiation from a wellbore in transversely isotropic rock. In: ARMA 11–201, Proc. 45th US Rock Mechanics/Geomechanics Symposium, San Francisco, CA, USA.
Sone, H., 2012. Mechanical Properties of Shale Gas Reservoir Rocks and its Relation to the In-situ Stress Variation Observed in Shale Gas Reservoirs. Ph.D. Thesis. Standford University, Stanford, California.
Spalletti, L.A., Franzese, J.R., Matheos, S.D., Schwarz, E., 2000. Sequence stratigraphy of a tidally dominated carbonate–siliciclastic ramp; the Tithonian–Early Berriasian of the Southern Neuquén Basin, Argentina. J. Geol. Soc. 157 (2), 433–446.
Stinco, L., Barredo, S., 2014a. Vaca Muerta Formation: an Example of Shale Heterogeneities Controlling Hydrocarbon's Accumulations. Unconventional Resources Technology Conference (URTeC). Denver, Colorado, USA. American Association of Petroleum Geologists.
Stinco, L., Mosquera, A., 2003. Estimación del contenido total de carbono orgánico a partir de registros de pozo para las formaciones Vaca Muerta y Los Molles, Cuenca Neuquina, Argentina. In: II Congreso de Hidrocarburos. IAPG, Buenos Aires, Argentina.
Suarez-Rivera, R., Deenadayalu, C., Chertov, M., Hartanto, R.N., Gathogo, P., Kunjir, R., 2011. Improving Horizontal Completions on Heterogeneous Tight-shales. Society of Petroleum Engineers. http://dx.doi.org/10.2118/146998-MS (2011, January 1).
Thomsen, L., 1986. Weak elastic anisotropy. Geophysics 51 (10), 1954–1966 (October 1986).
Thorne, L., Wallace, C., 1995. Modern Global Seismology. Chapter 2: Elasticity and Seismic Waves (Page 50).
Tutuncu, A., 2010. Anisotropy, compaction and dispersion characteristics of reservoir and seal shales. In: ARMA 10–344, Proc. 44th US Rock Mechanics/Geomechanics Symposium, Sal Lake City, USA.
Tutuncu, A., 2012. The role of mechanical, acoustic and permeability anisotropies on reservoir characterization and field development for two North American fractured unconventional shale reservoirs. In: ARMA 12–664, Proc. 46th US Rock Mechanics/Geomechanics Symposium, Chicago, USA.
Tutuncu, A., Mese, A., 2011. Relationship between permeability, acoustic, mechanical and strength anisotropies in unconventional reservoirs and sea shales. In: ARMA 11–532, Proc. 45th US Rock Mechanics/Geomechanics Symposium, San Francisco, USA.
Vernik, L., Nur, A., 1992. Ultrasonic velocity and anisotropy of hydrocarbon source rocks. Geophysics 57 (5), 727–735.
Voigt, W., 1928. Lehrbuch der Kristallphysik, reprient of the 1st Ed. Leizig, Teubner.
Wang, Z.Z., 2000. Dynamic versus static elastic properties of reservoir rocks. In: Wang, Z., Nur, A. (Eds.), Seismic and Acoustic Velocities in Reservoir Rocks: Recent Developments. Society of Exploration Geophysicists, Tulsa, Oklahoma, pp. 531–539.
Wang, Z.Z., 2001. Fundamentals of seismic rock physics. Geophysics 66 (No. 2).
Wang, Z.Z., 2002. Seismic anisotropy in sedimentary rocks, part 2: laboratory data. Geophysics 67 (5), 1423–1440.
Warpinski, N.R., Peterson, R.E., Branagan, P.T., Engler, B.P., Wolhart, S.L., 1998. In situ stress and moduli: comparison of values derived from multiple techniques. In: Paper SPE 49190 Presented at the 1998 SPE Annual Technical Conference and Exhibition Held in New Orleans, Loisiana, 27–30 September 1998.
Willis, M., Tutuncu, A., 2014. Integration of core drilling, microseismic and well log data for geomechanical property determination and monitoring in the Argentinian Vaca Muerta shale formation. In: UnconventionalResources Technology Conference, Denver, Colorado, USA, 25-27, 2014. URTeC 1922481.
Winkler, K.W., Sinha, B.K., Plona, T.J., 1998. Effects of borehole stress concentrations on dipole anisotropy measurements. Geophysics 63 (1), 11–17.
Zoback, M.D., Byerlee, J.D., 1975. The effect of cyclic differential stress on dilatancy in westerly granite under uniaxial and triaxial conditions. J. Geophys. Res. 80, 1526–1530.